UCRL-11531
corrected

University of California

Ernest O. Lawrence Radiation Laboratory

MUON CAPTURE IN OXYGEN

Berkeley, California

DISCLAIMER

UNIVERSITY OF CALIFORNIA
Lawrence Radiation Laboratory
Berkeley, California

AEC Contract No. W-7405-eng-48

August 31, 1964

ERRATA

TO: All recipients of UCRL-11531

FROM: Technical Information Division

Subject: "Muon Capture in Oxygen," by David Albert Jenkins (Ph. D. Thesis), June 29, 1964.

Please replace the attached pages in subject report. The pages with changes on them are 40, 47, 48, 50, and 52.

UCRL-11531

UNIVERSITY OF CALIFORNIA

Lawrence Radiation Laboratory
Berkeley, California

AEC Contract No. W-7405-eng-48

MUON CAPTURE IN OXYGEN

David Albert Jenkins

(Ph. D. Thesis)

June 29, 1964

Printed in USA. Price $1.75. Available from the
Office of Technical Services
U. S. Department of Commerce
Washington 25, D.C.

MUON CAPTURE IN OXYGEN

Contents

MUON CAPTURE IN OXYGEN

David Albert Jenkins

Lawrence Radiation Laboratory
University of California
Berkeley, California

July 1, 1964

ABSTRACT

The muon-capture rate in oxygen, $\mu^- + O^{16} \rightarrow N^{16*} + \nu$, is used as a means for measuring the induced-pseudoscalar-coupling constant (C_P) of weak interactions. The capture rates between the $J^P = 0^+$ state of O^{16} and the 0^- and 1^- states of N^{16} are measured by the stopping of muons in water where some of them are captured by O^{16} and form excited states of N^{16}. Capture into the excited states of N^{16} is identified by counting the gamma rays that are emitted in the nuclear transition to the ground state. We measure a rate of $(1.6 \pm 0.2) \times 10^3$ sec^{-1} for the capture rate into the 0^- state. Using this rate, we calculate C_P with different nuclear models for the O^{16} wave functions. We find that the transition rate, and therefore C_P, depends strongly on the nuclear model. We conclude that $5 < C_P/C_A < 20$.

I. INTRODUCTION

Muon capture in oxygen to bound states of nitrogen

$$\mu^- + O^{16} \rightarrow N^{16*} + \nu$$

has been suggested as a measure of the induced-pseudoscalar-coupling constant C_P of weak interactions.[1] This constant is of interest because its presence can be predicted on the basis of general invariance conditions and its magnitude can be calculated approximately. It enters into the capture rate via the Hamiltonian for the weak interactions:

$$\mathcal{H} = \left[\overline{\psi}_a(g_V + \gamma_5 g_A)\gamma_\mu \psi_b\right] \overline{\psi}_\ell \gamma_\mu (1 + \gamma_5)\psi_\nu$$

for the reaction $a + \ell \rightarrow b + \nu$, where ℓ refers to the lepton involved in the interaction, g_V is the vector-coupling constant, g_A is the axial-vector-coupling constant, and γ_5 and γ_μ are Dirac matrices. For muon decay, $g_V = -g_A$, and a measurement of the decay rate allows a straightforward calculation of the coupling constant g_V. However, when strongly interacting particles participate in reactions such as beta decay and muon capture, the Hamiltonian must be extended because of the virtual process

$$p \leftrightarrow n + \pi .$$

The axial part of the Hamiltonian is written

$$\mathcal{H}^A = \left[\overline{\psi}_n \gamma_5 g_A \gamma_\mu \psi_p\right] \overline{\psi}_\ell \gamma_\mu (1 + \gamma_5)\psi_\nu$$

where g_A is now an unrenormalized coupling constant. Following the method of Goldberger and Treiman, the general form for the Hamiltonian can be written

$$\mathcal{H}^A = \overline{\psi}_n \left(C_A\, i\gamma_5 \gamma_\mu + C_P \frac{q_\mu}{m_\mu}\right) \psi_P \overline{\psi}_\ell \gamma_\mu (1 + \gamma_5)\psi_\nu ,$$

where the coupling constants C_A and C_P are functions of the square of the lepton momentum q. The constant C_P is induced into the interaction by the presence of the strongly interacting particles, hence the name "induced-pseudoscalar-coupling constant."

This form of the Hamiltonian is the result of considering all variables that contribute to an axial-vector current, are Lorentz invariant, and have the proper transformation properties under G conjugation. In the limit $q \to 0$, $C_A = g_A$. The problem is to evaluate the coupling constants C_A and C_P and to compare the results with those obtained experimentally.

Goldberger and Treiman have computed these coupling constants using dispersion relations.[2] However the same constants can be computed in several different ways that give approximately the same result. In one derivation[3] the nucleon part of the interaction is treated as a current J_μ with the matrix element

$$\left\langle n \left| J_\mu \right| p \right\rangle = \overline{\psi}_n \left(i C_A(q^2)\, \gamma_\mu \gamma_5 + C_P(q^2)\, \frac{q_\mu}{m_\mu}\, \gamma_5 \right) \psi_p \ .$$

Now the matrix element for the divergence of the current is

$$\left\langle n \left| \frac{\partial J_\mu^A}{\partial x_\mu} \right| p \right\rangle = i(2M\, C_A - \frac{q^2}{m_\mu}\, C_P)\ \overline{\psi}_n \gamma_5 \psi_p,$$

since

$$\frac{\partial J}{\partial x_\mu} = i\,[p_\mu, J] \quad \text{and} \quad \gamma_\mu p_\mu = im.$$

Here M is the nucleon mass.

We now assume that the matrix element will satisfy a dispersion relation with a dominant term from the one-pion exchange, as shown:

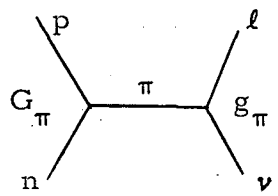

The contribution of the exchange to beta decay is small since the decay $\pi \rightarrow e + \nu$ is down by 10^{-4} compared with the normal decay $\pi \rightarrow \mu + \nu$. With dispersion theory, the one-pion pole term leads to

$$\left\langle n \left| \frac{\partial J_\mu^A}{\partial x_\mu} \right| p \right\rangle = -i\sqrt{2} \frac{G_\pi g_\pi m_\pi^2}{q^2 + m_\pi^2} \bar{\psi}_\mu \gamma_5 \psi_p,$$

where G_π is the strong-interaction pion-nucleon coupling constant and g_π is the coupling constant for π decay. Equating these two relations yields

$$2M C_A(q^2) - \frac{q^2}{m_\mu} C_P(q^2) = \frac{-\sqrt{2} G_\pi g_\pi m_\pi^2}{q^2 + m_\pi^2} . \qquad (1)$$

Then for $q^2 = 0$, this equation gives

$$2 M C_A(0) = -\sqrt{2} G_\pi g_\pi,$$

which is called the Goldberger-Treiman relation. Using

$$g_\pi = 1.48 \times 10^{-7} m_\pi^{-1} \qquad \text{(Ref. 4, p. 468) and}$$

$$\frac{G_\pi^2}{4\pi} \approx 13.5 \qquad \text{(Ref. 5, p. 315),}$$

we can calculate C_A

$$C_A(0) = -0.91 \times 10^{-5} M^{-2} \qquad \text{(calculated).}$$

Now assume that $C_A(q^2) = C_A(0)$, substitute for $G_\pi g_\pi$ in Eq. (1), and solve for C_P

$$C_P(q^2) = \frac{2M m_\mu C_A(0)}{q^2 + m_\pi^2}$$

$$\approx 6.5 C_A.$$

Taylor has estimated the corrections from high mass states and he concluded the C_P must be between 6.5 and 7.5 if the Goldberger-Treiman relation is valid.[6]

We now have values for C_A and C_P that can be compared with experimental values. In beta decay the effect of C_P is so small that it can be ignored. One then obtains a value for C_A from the beta decay of the neutron and O^{14} (Ref. 5)

$$C_A = -1.23 \times 10^{-5} \ M^{-2} \text{ (experimental)},$$

which is within 24% of the computed value; considering the nature of the many approximations, the agreement is surprisingly good.

With C_A determined by beta decay, C_P can be measured in a muon-capture reaction and can be obtained directly from a measurement of the muon-capture rate in hydrogen. However the measurement is experimentally difficult because of the formation of the $p\mu p$ molecule when muons stop in liquid hydrogen. Therefore one observes capture in complex nuclei and hopes that knowledge of the nuclear physics of the reaction will allow a determination of the muon-proton interaction. Experimental evidence for the existence of a pseudoscalar interaction comes from the observation[7] of (a) the angular distribution of neutrons following capture of polarized muons, (b) the muon-capture rates in H, He^3, and C^{12}, and (c) the results of radiative capture in Ca^{40}. Unfortunately, these experiments do not provide a precise measurement of C_P because of the uncertainty in the initial and final-state wave functions. For a precise measurement, one needs a muon-capture transition in which the matrix element for the pseudoscalar coupling is large relative to the other matrix elements, and in which the initial- and final-nuclear-wave functions are accurately known. The muon-capture rate between the $J^P = 0^+$ ground state of O^{16} and the $J^P = 0^-$ state of N^{16} satisfies both of these criteria reasonably well. For a $0^+ \rightarrow 0^-$ transition, there is no contribution from the vector part of the weak-interaction Hamiltonian, and the matrix element for the axial-vector coupling has the same magnitude as the pseudoscalar-

matrix element. Furthermore, since O^{16} has a closed-shell nucleus, the wave functions should be well known.

The purpose of the present work is to measure C_P by means of the $0^+ \rightarrow 0^-$ transition in O^{16}. Section II describes a measurement of the muon-capture rate in O^{16}. In Section III the transition rate is calculated as a function of C_P, and in Section IV the conclusions are presented.

II. EXPERIMENT

A. Capture-Rate Measurement in O^{16}

In order to determine muon-capture rates in O^{16}, muons are stopped in water where some of them are captured by the O^{16} nucleus and form N^{16}. With 105-MeV available energy, the N^{16} nucleus can be in any excited state; but only the bound states are of interest, and these are shown in Fig. 1. There are only four bound states observed[8] in N^{16}. Capture into the $J^P = 0^-$ state is identified by observation of the 120-keV gamma ray that is emitted in the 0^- to ground-state transition following capture. However, the 0^- state is fed by both direct capture and cascade gamma rays from the 1^- level. Capture in higher excited states is ignored since these states are above the neutron-emission threshold, and their mean life is too short to permit any gamma branching. The transition rate into the 0^- state is then found by measuring the number of (a) muons stopped in O^{16}, (b) 276-keV gamma rays (1^- to 0^- transition), and (c) 120-keV gamma rays (0^- to ground state) emitted.

The capture rate in O^{16} has been measured by a group at Columbia University with a different experimental method,[9] but their results compare reasonably with the results of this experiment.

B. Beam and Target Arrangement

The beam layout is shown in Fig. 2. A beam of pions, muons, and electrons is produced by protons striking a beryllium target in the Berkeley 184-inch cyclotron. The beam is momentum analyzed by the cyclotron field and focused by an 8-inch quadrupole magnet. The resulting 180-MeV/c beam passes through the meson wheel in the cyclotron shielding and is moderated to 110 MeV/c by 11 inches of polyethylene degrader. Muons in the beam are then identified by a time-of-flight system. This beam was used in a measurement of the muon-capture rate in He^3 (Ref. 10), and this reference should be consulted for a more detailed description.

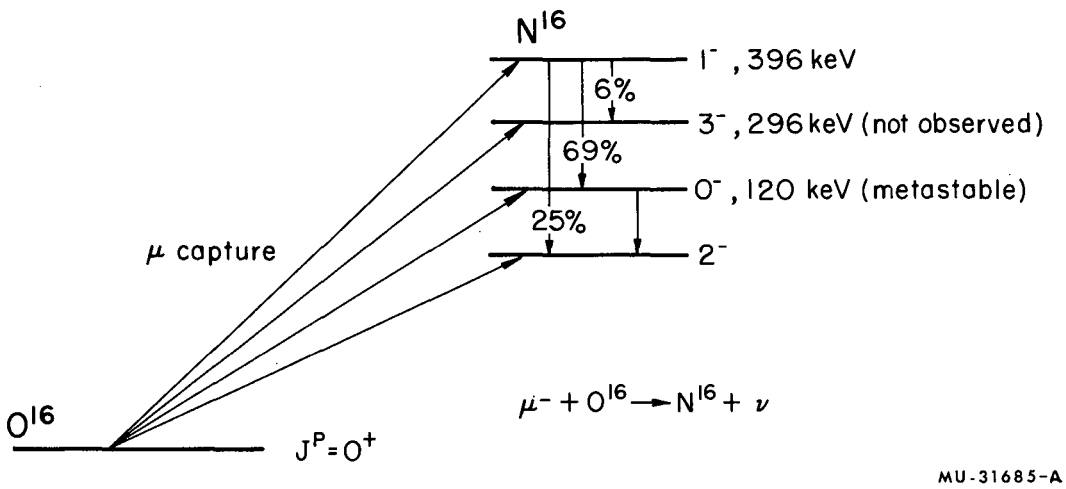

Fig. 1. Level and decay scheme for the muon-capture reaction in O^{16}.

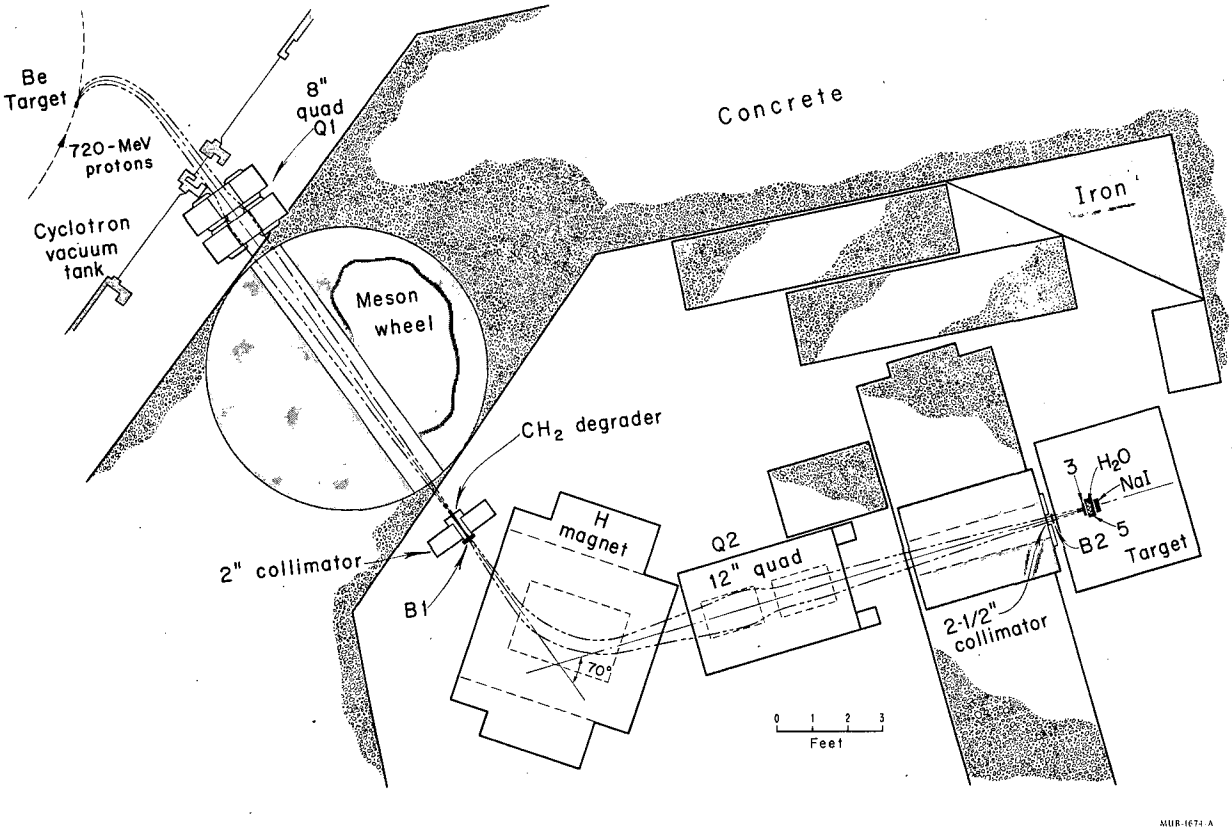

Fig. 2. Muon-beam arrangement.

After being identified by the time-of-flight system, the muons pass through a counter (No. 3) and are brought to rest in a water cell 1-inch thick and 2.5 inches in diameter, as shown in Fig. 3. The water cell was made from the scintillator material that comprised counter No. 5, and a small layer (1/32 inch) of Lucite (not shown in Fig. 3) covered the front end of the cup so as to contain the water within the No. 5 cup counter. A NaI counter, placed in the beam behind the water cell to detect gamma rays emitted in the N^{16} nuclear transitions, was kept near the water to maximize the solid angle subtended by the water cell and thereby increase the counter efficiency.

Since we assumed the background would be proportional to the volume of the crystal, we chose small NaI crystals. Two different NaI crystals were used while data were being taken; both crystals were 2.5 inches in diameter but one was 1/4-inch thick and the other was 1-inch thick. The crystals were obtained from the Harshaw Chemical Company (Type HA) and were mounted on Dumont 6363 phototubes. Counter 3 consisted of a scintillator 2.5 inches in diameter and 1/16-inch thick, and counter 5 was a cup made from a scintillator 1/4-inch thick on all sides. Counters 3 and 5 were both mounted on RCA 6810A tubes; counter 5 was mounted on two tubes to increase its detection efficiency. These two counters were juxtaposed so that no particle could enter or leave the water cell without passing through one of them.

There were 800 particles/second in the beam analyzed by the time-of-flight system. Of these, 64% were identified as muons and 58% of the muons stopped in the water cell.

C. Electronics

In setting up the electronics, we made use of the metastable property of the 0^- level of N^{16}. The 0^- state has a mean life of 8.26 μsec, [11] and the background problem was simplified by collecting the NaI data in four different time intervals during the

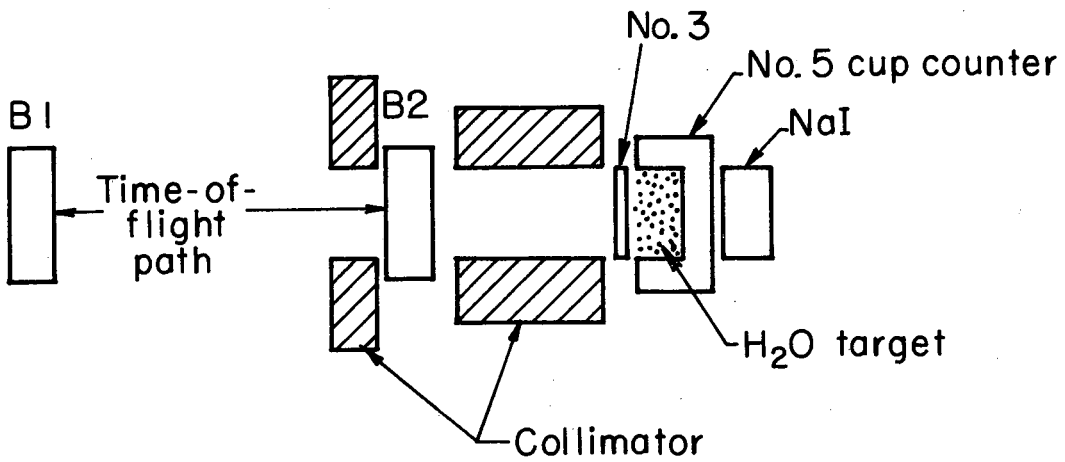

Fig. 3. Counter arrangement for measuring capture rates.

0^- decay. The background present during the 1^- to 0^- transition was reduced by requiring a delayed coincidence between the 276-keV gamma ray emitted and the 120-keV gamma ray that follows.

Figure 4, which gives a logic diagram of the electronics used in the experiment, has been abbreviated for the sake of clarity. A muon in the beam (B_μ) was signalled by a coincidence between counters B1 and B2 with the proper timing in the time-of-flight system. A muon stopping in the water cell (S_μ) was signalled by the presence of counts from B_μ and counter 3 and the absence of a count in counter 5.

The electronic logic required about 42 μsec to analyze an event with the coincidence system, and the analysis of an event could become confused if a second B_μ pulse should arrive at S_μ within 42 μsec of the arrival of the first B_μ pulse. Therefore the S_μ signal was disabled by the inhibit pulse (shown in Fig. 4) for 50 μsec after receiving a B_μ signal.

The signal from a stopped muon fired five delay-and-gate units, each of which generated a pulse 4 μsec long. The pulses were arranged in time to give four equal-time intervals from 0 to 16 μsec and one from 30 to 34 μsec after the muon had been stopped (see timing sequence shown in Fig. 4). We called the time intervals τ_1, τ_2, τ_3, τ_4, and τ_5. The fifth time interval was delayed many muon lifetimes so that all pulses in that time interval could be considered as a random background; τ_5 was used in the background analysis. The first time interval was delayed 0.45 μsec to make absolutely certain that a 133-keV mu-mesic x ray from O^{16} could not be detected as a capture gamma ray. Intervals τ_1 and τ_2 were separated by 0.20 μsec to prevent one pulse from counting in both τ_1 and τ_2, thereby interfering with a coincidence circuit described below. The water target was completely surrounded by plastic scintillator and, if a decay electron from the stopped muon were detected between 0 and 11 μsec, the muon was rejected by a μ-e logic system not shown in Fig. 4. The μ-e logic system is described in Ref. 9.

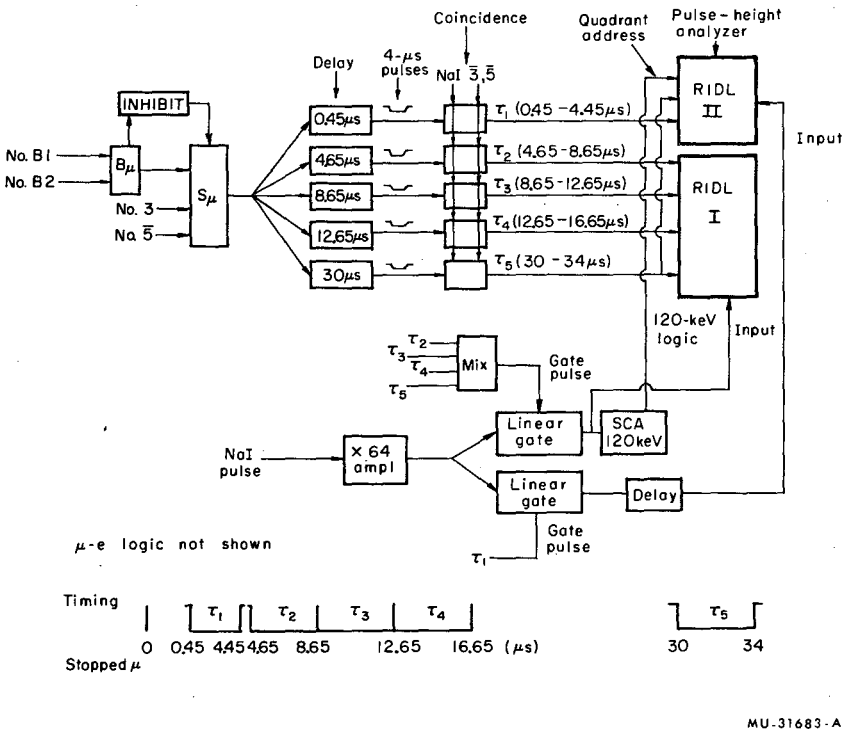

Fig. 4. Electronic arrangement and timing sequence for counting gamma rays from excited states of N^{16}.

The pulse-height data from the NaI detector was collected on two RIDL (Radiation Instrument Development Laboratory, Inc.) 400-channel analyzers each with its memory split into four sections. A coincidence between one of the 4-μsec gates and a fast NaI pulse with no count in counters 3 or 5 produced a trigger for a 0.60-μsec linear gate and a routing pulse. The slow pulse from the NaI was accepted by the linear gate and was directed by the routing pulse to the appropriate region of the analyzer. Pulses in τ_2, τ_3, τ_4, and τ_5 routed the slow NaI pulse to sections of RIDL I and a pulse in τ_1 directed the slow NaI pulse to RIDL II. In this way, pulse-height spectra were obtained for five different time intervals, as shown in Sec. II. E.

The number of 276-keV gamma rays emitted was measured with a delayed coincidence between a NaI count in τ_1 and a 120-keV gamma ray in τ_2, τ_3, or τ_4. The idea of the coincidence is to signal an event in τ_1, which is followed by a 120-keV gamma ray in τ_2, τ_3, or τ_4. Figure 4 shows that pulses in intervals τ_2, τ_3, τ_4, and τ_5 opened a linear gate whose output was divided. One part went to RIDL I, which recorded the spectrum; the second part was directed to a single-channel analyzer, which gave an output when a 120-keV gamma ray was seen. The output from the single-channel analyzer served as a routing pulse that superseded the τ_1 routing pulse and stored pulses for the first 4 μsec in a different section (called τ_{logic}) of RIDL II. Of course, if there were no pulse in the NaI during the first 4 μsec when a 120-keV pulse in τ_2, τ_3, τ_4, or τ_5 was received, nothing was stored in τ_{logic}. Not shown in the diagram is a circuit that voided the address from the 120-keV logic if it was derived from a pulse in τ_5. The end result is a τ_{logic} spectrum representing those pulses in the NaI that appear between 0.45 and 4.45 μsec and are followed by a 120-keV pulse in τ_2, τ_3, or τ_4. The spectrum is shown in Sec. II. E.

D. Calibrations

Mesic x rays and gamma emitters of known intensity were used to find the efficiency of the system for detecting a gamma ray in the photopeak of the NaI crystal. Mesic x rays provided the best measurement of the efficiency, but as x rays of the correct energy could not be found we used both methods and compared the results.

Mesic x rays are emitted for every muon that stops in a substance, and a list of K x-ray energies for the different materials used in our calibrations is shown in Table I.[12] In calibrating the NaI with mesic K x rays from O^{16}, we employed the water cell in the same target arrangement used for taking data. Therefore the calibration was easily obtained after a small change in the electronics.

Table I. Mesic K_α x-ray energies.[a]

Element	Energy (keV)
Oxygen	133.1
Sodium	249.0
Magnesium	294.4
Aluminum	344.3
Silicon	397.0

[a]K. W. Ford and J. G. Wills, Calculated Properties of Mu-mesic Atoms, LAMS-2387, March 1, 1960; Nucl. Phys. 35, 295 (1962).

To take mesic x-ray calibrations with other materials, the water cell was removed and the new material was substituted for the water. The thickness of the new material was chosen so that it would have the same attenuation power as water for the given x-ray energy. Then the spectrum was taken on the pulse-height analyzer with an electronics arrangement similar to that in Fig. 4, except that a prompt coincidence was required between S_μ and the NaI pulse rather than a delayed coincidence.

A typical x-ray spectrum is shown in Fig. 5 where three peaks occur in the spectrum. The middle peak at 133 keV is the photopeak representaing a K_α x ray that has lost all of its energy in the NaI crystal; the lower peak is the escape peak and the higher one is produced by K_β and higher energy x rays from muons that fall into the K shell without passing through the L shell. The higher peak can also be due to a muon's L and K_α x rays both entering the NaI crystal and thereby increasing the total energy deposited in the crystal. As a result, the K_α x ray will not appear in the photopeak. The fraction of x rays that falls into the upper peak must be estimated before the efficiency can be computed;[13] however, the final efficiency is not sensitive to this fraction. Background under the peak is probably due to muon decays and captures that follow the emission of an x ray. Since the x ray is emitted within 10^{-9} sec[14] after stopping and the decay and capture occur about 2 μsec after stopping, most of the background could be removed by use of a very short S_μ pulse in coincidence with the NaI. However we found that we could not make the coincidence narrow enough to eliminate the background, so we took mesic x-ray spectra for a range of S_μ pulse lengths and extrapolated to zero length. We then assume that all of the background is eliminated.

We discovered that the efficiency depends on energy and, because we could not find mesic x rays of 120 and 276 keV, we used sources that emitted gamma rays of the proper energy. To calibrate the NaI crystal with a gamma source of known intensity, the water target is replaced with a water solution in which the gamma-emitting substance has been dissolved.

We used the sources listed in Table II to find the energy dependence of the efficiency.[15] The Co^{57} and Hg^{203} sources had the correct energies and would allow an accurate measurement of the efficiency if they had the proper geometry. Unfortunately the sources emit gamma rays uniformly throughout the water solution in which they are dissolved. But in the actual experiment, muons tend to be stopped and captured in the center of the water cell; as a result the gammas are emitted nonuniformly in the water cell when a muon is

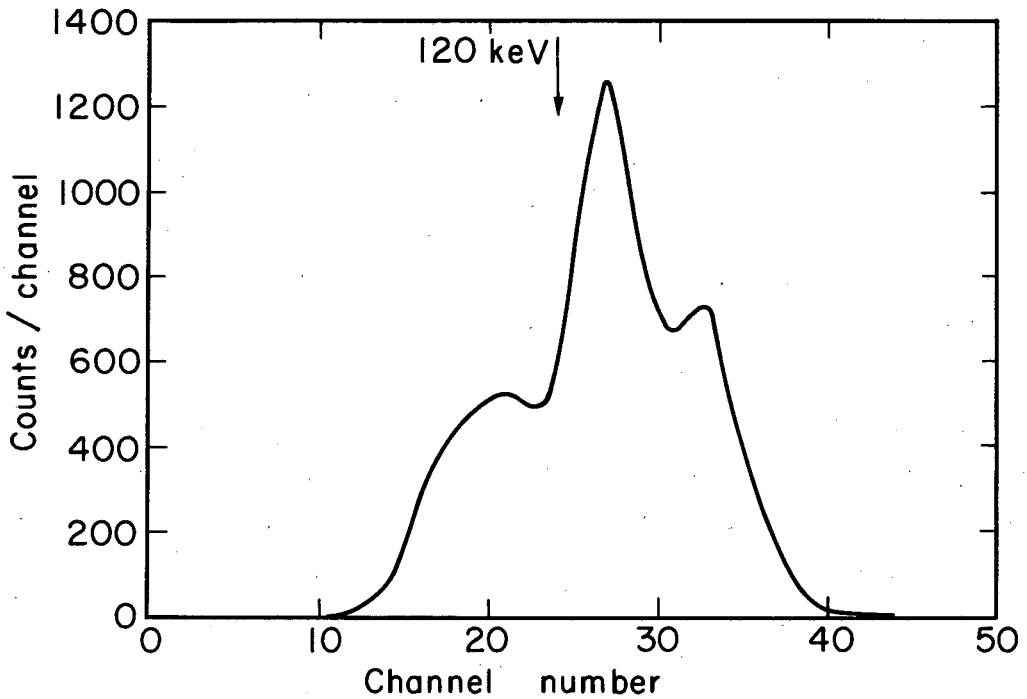

Fig. 5. Mesic x-ray spectra for muons stopping in O^{16}.

Table II. Gamma-ray energies.

Nucleus	Energy (keV)
Co^{57}	122
Hg^{203}	279
Cr^{51}	323
Ba^{133}	380
Be^{7}	477

captured. For this reason, the calibrated gamma emitters do not give the same efficiency as required for the experiment. Some calculations can be made to correct for the difference, but their validity is questionable since there are many side effects for gamma detection in NaI crystals.

Figure 6 shows the efficiency as a function of energy for the two different methods taken for one group of data (run No. 3 described in Sec. II. E). The two methods of calibration give good agreement, so we have confidence that the efficiency is known to an accuracy of 5%.

E. Data and Results

In the data analysis, we subtracted the background beneath the photopeaks in the pulse-height spectrum. An analysis of the pulse-height spectrum shown in Fig. 7 for the first 4 μsec is difficult because of the high number of background counts. The background arises from the high-energy products of muon capture in O^{16} that deposit only part of their energy in the NaI. We expect a large contribution from these high-energy processes because our NaI crystal is gated open for every muon-capture event and only 2% of these captures lead to bound states of O^{16}. The background has the lifetime characteristic of a muon in O^{16} (1.81 μsec[4]), and most of it will have disappeared after the first 4 μsec. The metastable character

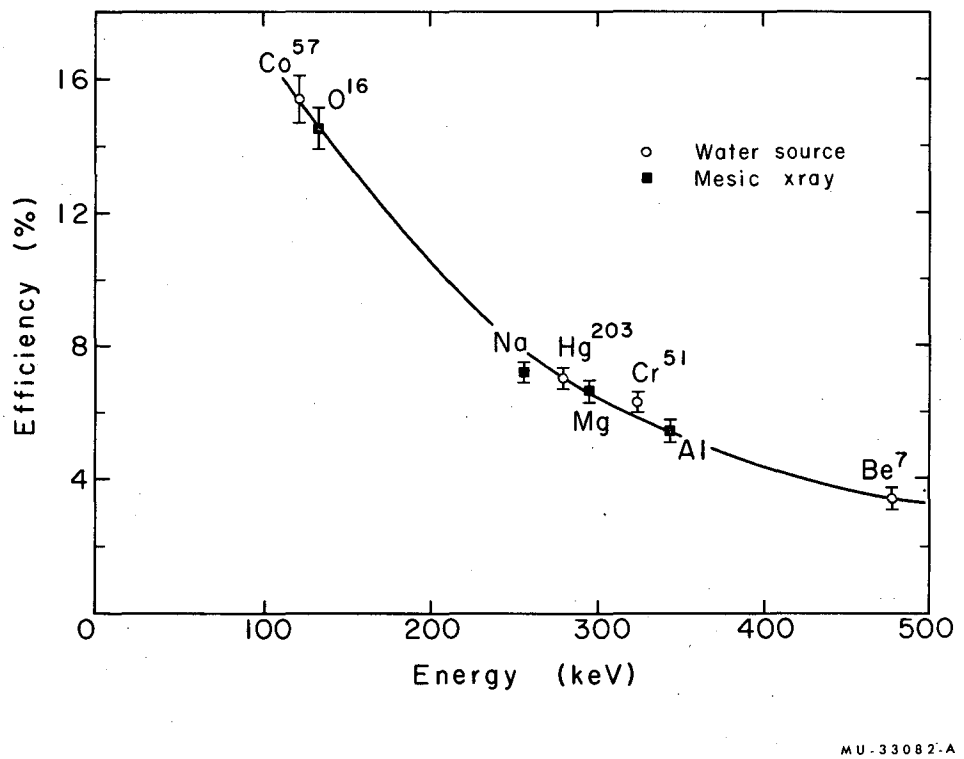

Fig. 6. NaI counter efficiency.

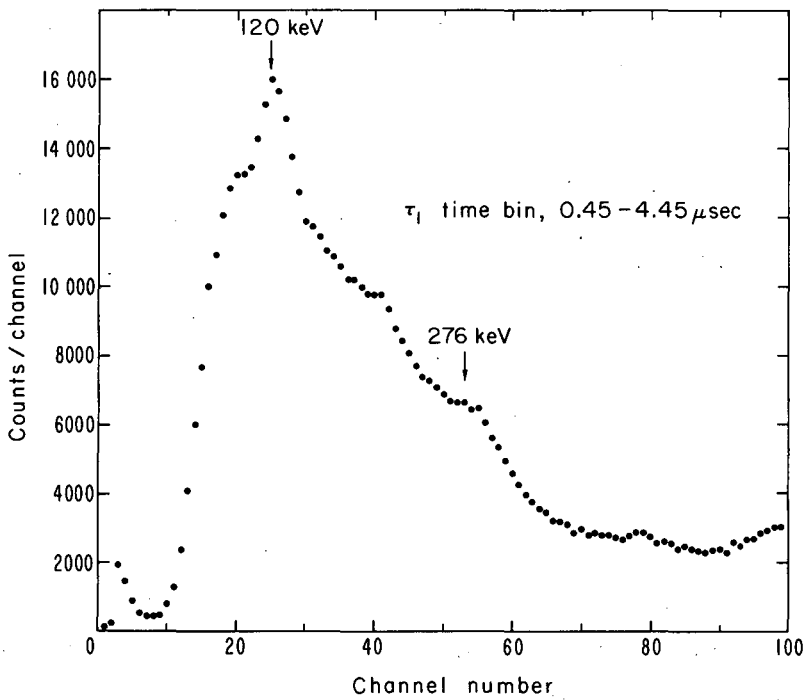

Fig. 7. Pulse-height distribution in NaI counter.

of the 0^- state was used to detect the 120-keV gamma ray. Only 28% of the nuclei in the 0^- level will have decayed during the first 4.45 μsec; and, by waiting for the time intervals τ_2, τ_3, and τ_4, we find that most of the background has disappeared and the 120-keV peak dominates, as shown in Fig. 8. Note that the small peak below the 120-keV photopeak is an escape peak. The background decreases with a mean life of 1.81 μsec while the 120-keV peak rises and falls with a mean life of 8.26 μsec.

We divide the background into two categories. The first type, called a target-derived background, is produced by the high-energy decay products of N^{16}. It is assumed to have the characteristic muon mean life of 1.81 μsec. The second type of background is called a random background and should be independent of the muon's stopping in the target. The random background probably came from the cyclotron and we assume that it would be the same for any 4-μsec interval.

The target-derived background is negligible in the τ_5 spectra since most of the capture products will have decayed before this time interval, but there is a small peak due to the 120-keV gamma. The 120-keV peak can be removed, and the τ_5 spectrum is then used as a measurement of the random background, which can now be subtracted from the τ_1, τ_2, τ_3, and τ_4 spectra. The background remaining in time intervals τ_3 and τ_4 is a target-derived background whose shape can be derived from τ_1 and which can then be subtracted from τ_3 and τ_4. However the target-derived background makes only a small contribution to τ_3 and τ_4. An example of the background subtraction is shown in Fig. 9, and Appendix A shows the mathematical details required for the subtraction. We did not use the data in τ_2 for the analysis of the 120-keV peak because the background was much higher for this time interval. However, the results from τ_2 agreed to within 10% with the results from τ_3 and τ_4. This disagreement could be attributed to an error in the mean life of the 0^- state, or it could be due to a bad background subtraction. The data in τ_3 and τ_4 were not

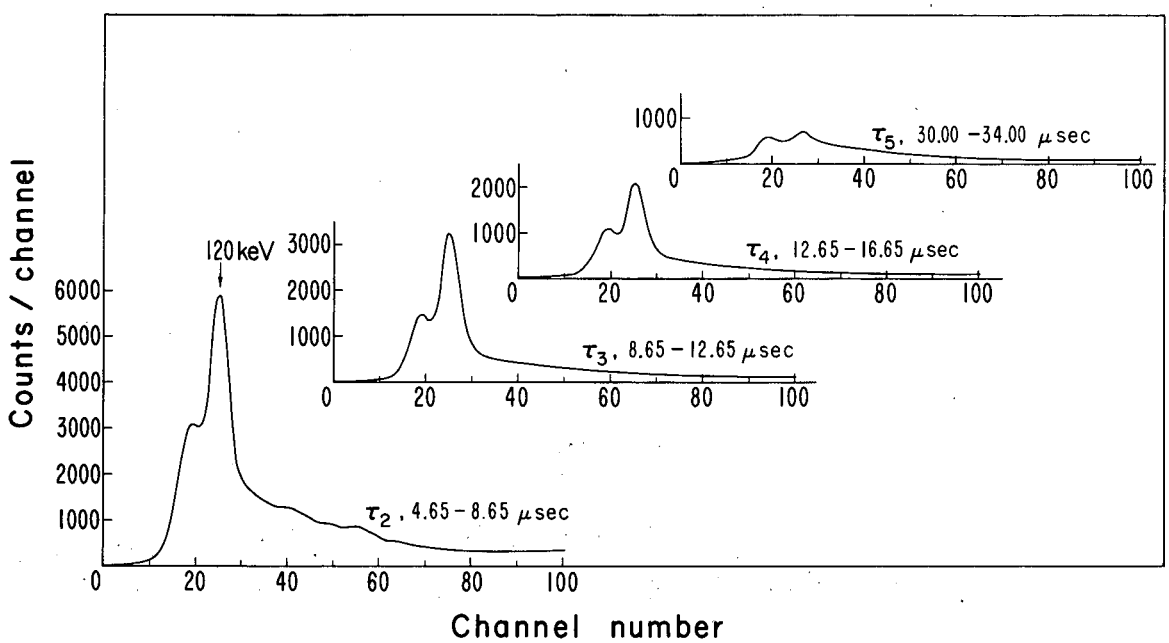

Fig. 8. Pulse-height distribution in NaI counter for different time intervals after a muon is captured.

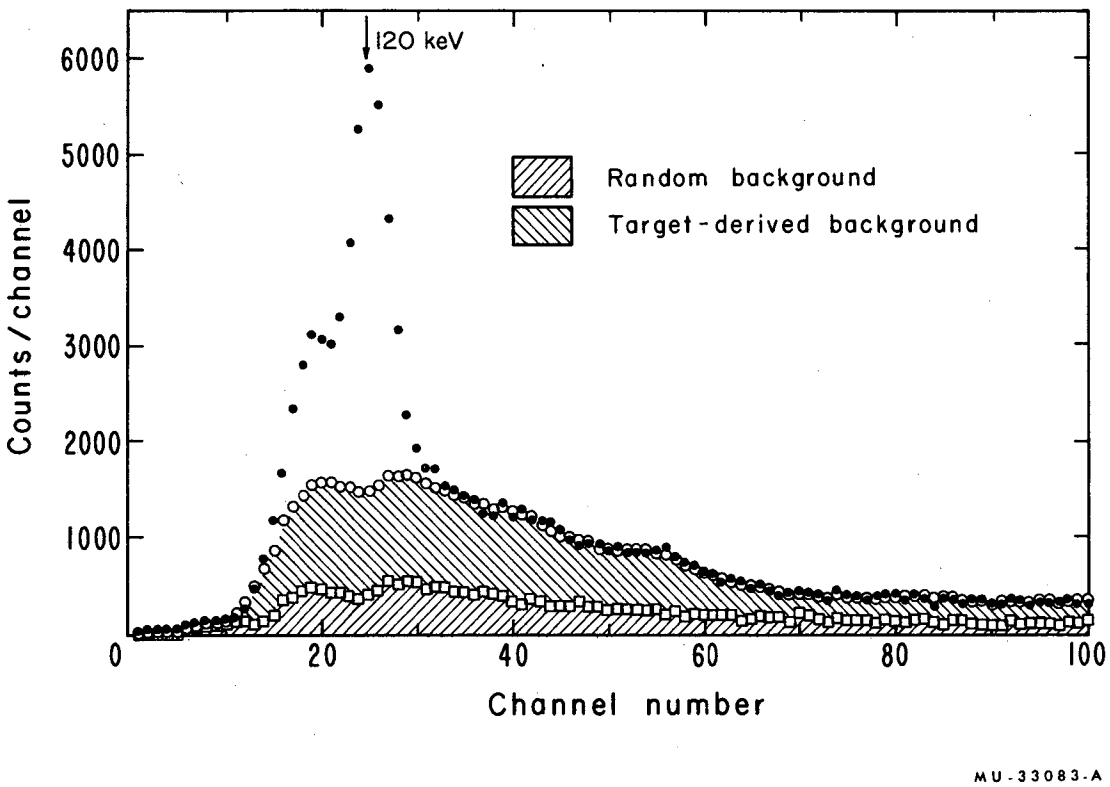

Fig. 9. Background subtraction for time interval τ_2.

sensitive to the 0^- mean life, and the uncertainty in the lifetime[11] introduces only a 3% error in the results. Once the subtractions are made, the 120-keV peak is obtained as shown in Fig. 10.

Data were taken in three separate groups as summarized in Table III. The symbols γ_{120}/S_μ represent the number of 120-keV gamma rays emitted per stopping muon. The background pulse-height spectrum τ_5 was not collected for the first two groups of data and part of the third, so the background was subtracted by fitting the shape of the background-pulse-height spectrum to τ_3 and τ_4. The efficiency of the NaI was different for the three runs because the geometry was altered slightly. Also, the number of stopping muons (S_μ) listed in Table III has been corrected to give the actual number of muons that stop in the water. The correction is necessary because muons could stop in either counter 3 or the Lucite cover on counter 5 and register as stopping muons; however this was only a 2% correction, as shown by a target-empty run. In addition, muons stopping in the walls of counter 5 may not have enough energy to initiate a veto pulse to S_μ, and these muons would then be counted as stopped muons. This correction is found by replacing the water by a copper target. Muons stopping in the copper will decay with a mean life of 0.164 μsec,[4] whereas muons stopping in carbon decay with a mean life of 2.026 μsec.[4] The fraction of muons that stop in carbon can be determined by first recording the time at which an electron is counted in counter 3 or 5 after a stopped muon has been counted. A decay curve is then drawn, and the muons that stop in copper and carbon can be separated by the different decay mean lives. We found that 2% of the muons were captured in carbon; some were captured in counter 3 and some in counter 5. Combining this correction with target-empty data, we find the number of stopped muons listed in Table III. It must be remembered that these corrections also apply to the mesic x-ray efficiencies, so that they tend to cancel when the mesic x-ray calibration is used.

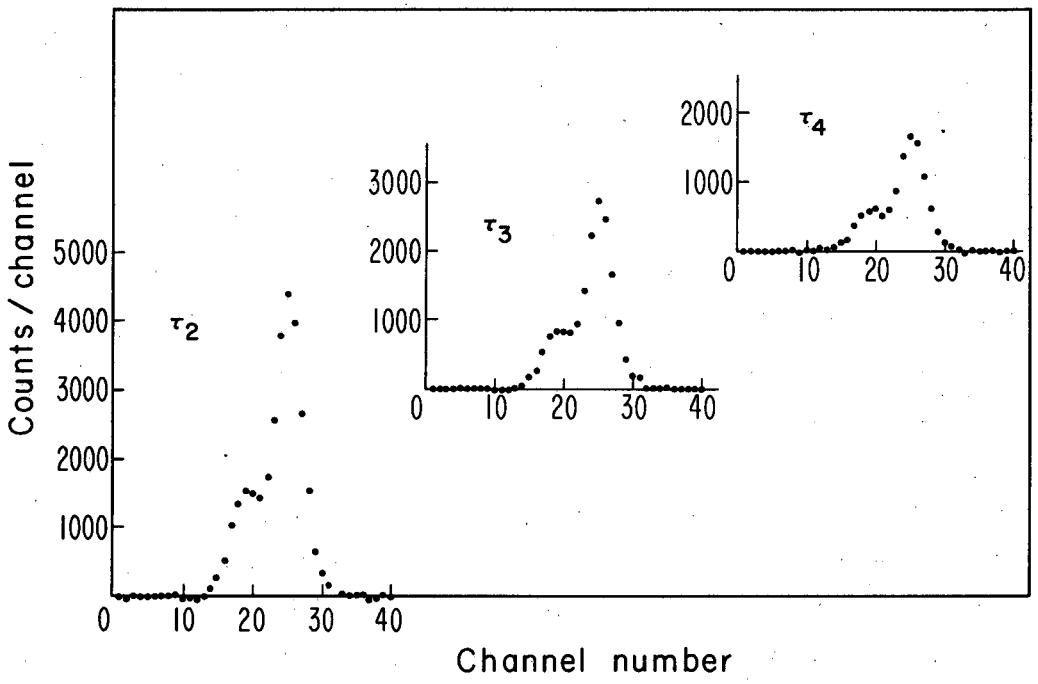

Fig. 10. NaI pulse-height distribution for the 120-keV gamma ray after background is subtracted.

Table III. Data for 120-keV gamma rays.

Run	NaI thickness (inch)	NaI efficiency	S_μ (in millions)	γ_{120}/S_μ (in hundredths)
1	0.25	0.145	49.1	0.48
2	1	0.136	64.9	0.44
3	1	0.154	147	0.45

A set of data was taken without the μ-e logic to make certain that the logic system was not affecting the results in some unknown manner, and this set of data is in good agreement with the Table III data. A 2.5% correction was made for γ_{120}/S_μ in Table III to account for events that have been vetoed by random pulses in the μ-e logic system.

The efficiency of the NaI (η) is used to give the number of 120-keV gammas (γ_{120}) per S_μ,

$$\frac{\gamma_{120}}{S_\mu} = \frac{N_{120}}{\eta_{120}\beta S_\mu} ,$$

where N_{120} is the number of γ_{120} in the pulse-height photopeak after background subtraction, and β is a time factor that accounts for the collection of N_{120} over a finite period of time. The time factor is derived in Appendix A.

The coincidence system was used while the third group of data was being taken and it determined the number of 276-keV gamma rays (γ_{276}) per γ_{120}.

$$\frac{\gamma_{276}}{\gamma_{120}} = \frac{N_{276}}{N_{120}\eta_{276}T_{276}}$$

$$= 0.38$$

where $\eta_{276} = 0.070$, N_{120} is the number of 120-keV gamma rays in τ_2, τ_3, and τ_4 that register in the single-channel analyzer as a 120-keV gamma, N_{276} is the number of 276-keV gamma rays counted under the photopeak of Fig. 11 after the background is subtracted, and T_{276} is the time factor derived in Appendix A.

When the above results are combined, the capture rate into the 0^- state per stopping muon can be computed

$$0^-/S_\mu = \frac{\gamma_{120}}{S_\mu} (1 - \gamma_{276}/\gamma_{120})$$

since

$$\frac{\gamma_{120}}{S_\mu} = 0^-/S_\mu + \gamma_{276}/S_\mu .$$

The background in τ_{logic} is not well understood and this contributed a large error to the final result. As shown in Fig. 11, there are 245 counts above channel 70 in the spectra and, if the spectra were due to a pure 276-keV gamma ray, these counts should not be present. When we made a background subtraction that seemed reasonable, 189 counts remained in the higher channels. Therefore we must admit that we do not understand the background, and we fit different shapes of background to the τ_{logic} spectra while requiring both the removal of all counts between channels 70 and 100 and a reasonable agreement with the shape of the Hg^{203} spectra. The result was 950 ± 50 counts in the 276-keV photopeak.

The number of captures into the 1^- level is easily found from the number of 276-keV gamma rays seen

$$1^-/S_\mu = \left(\frac{\gamma_{276}}{\gamma_{120}}\right)\left(\frac{\gamma_{120}}{S_\mu}\right) \frac{1}{a} ,$$

where a is the branching ratio of the 1^- level to the 0^- level and equals 0.69 ± 0.05.[8]

The data are combined to give the numbers shown in Table IV and the results are compared with a measurement made at Columbia

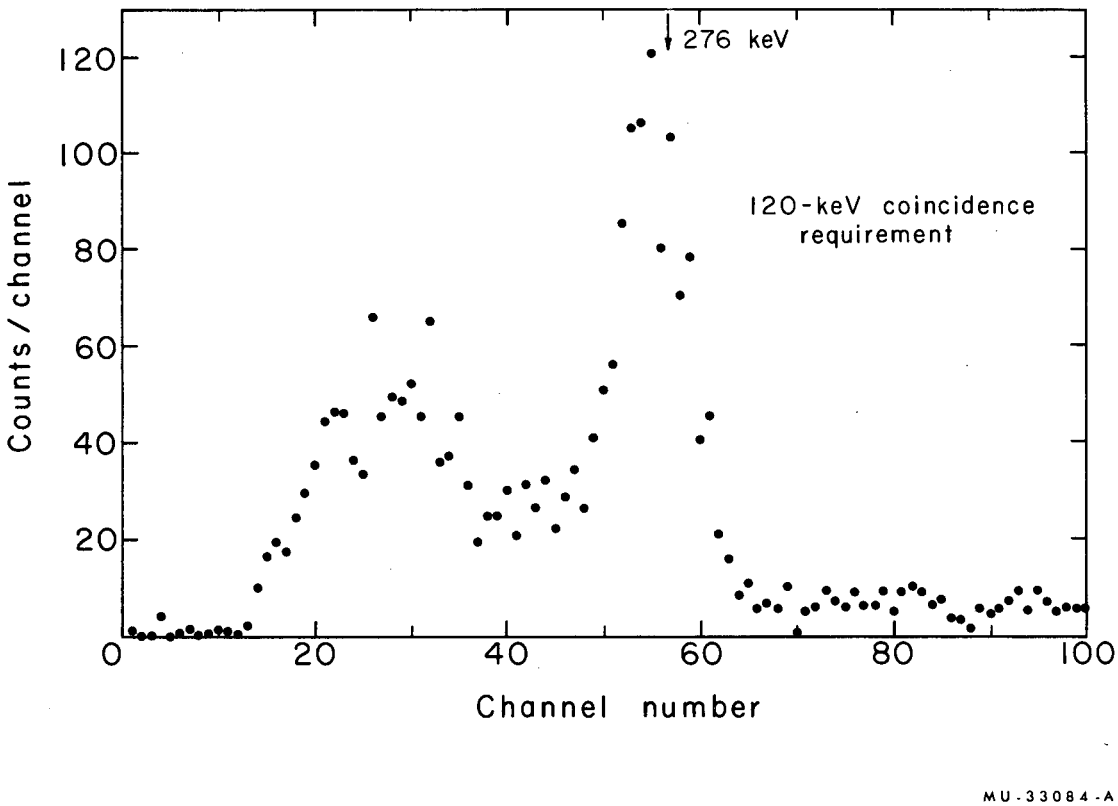

Fig. 11. Pulse-height distribution in the NaI for time interval τ_1 with the 120-keV coincidence requirement.

University. The biggest contribution to our errors came from the background subtraction in τ_{logic} and from the uncertainty in the NaI efficiency.

Table IV. Transition rates.

Transition	Data from this experiment	Data from Columbia University[a]
$0^-/S_\mu$	$(2.8 \pm 0.3) \times 10^{-3}$	$(1.9 \pm 0.3) \times 10^{-3}$
$1^-/S_\mu$	$(2.5 \pm 0.3) \times 10^{-3}$	$(3.14 \pm 0.18) \times 10^{-3}$
0^-	$(1.6 \pm 0.2) \times 10^{+3}$ sec^{-1}	$(1.1 \pm 0.2) \times 10^{3}$ sec^{-1}
1^-	$(1.4 \pm 0.2) \times 10^{+3}$ sec^{-1}	$(1.73 \pm 0.10) \times 10^{3}$ sec^{-1}

[a]Reference 9 uses a 1^- to 0^- branching ratio of 0.75.

The Columbia group did not use a coincidence system to find the 276-keV gamma ray. They reduced their background problem with an electronic system that stabilized the gain from their NaI pulse and allowed them to keep a uniform gain for long periods of time. As a result, their pulse-height spectra had good resolution and they could fit calibrated curves to the data in τ_1 to find the number of 276-keV gamma rays. However, without a coincidence system, this gamma can be confused with the 296-keV gamma ray emitted by the 3^- to 2^- transition (see Fig. 1). In Sec. III we find that the transition rate into the 3^- level is about 10% of the experimental rate into the 1^- level, and there is a 6% branching ratio for the 1^- to 3^- transition. If some of the 296-keV gamma rays were mistaken for 276-keV gamma rays, the apparent number of 276-keV gamma rays would be increased and the capture rate into the 0^- level would appear smaller.

The Columbia group used the shape-fitting method of background analysis in finding γ_{120}/S_μ. They also measured the capture rate into the 2^- ground state, which involves looking for a high-energy gamma ray over long periods of time, and we were not prepared to do

this. Nevertheless, the measurement is important since the capture rate into the 2^- state is also sensitive to the pseudoscalar-coupling constant.

In conclusions, the accuracy of our experiment is not as good as we desire, but a more accurate experiment is not justified until better wave functions for O^{16} can be found. As shown in the next section, the uncertainty in the O^{16} wave function introduces a large error into the determination of the pseudoscalar-coupling constant.

A more accurate measurement would also require better knowledge of the properties of the excited states of N^{16}. The lifetime of the 0^- state has been measured twice with two conflicting results,[11] and the 1^- to 0^- branching ratio is known to only 7% accuracy.[8]

III. CAPTURE-RATE CALCULATIONS

A. Muon Capture

When the universal Fermi interaction is assumed valid, muon-capture and beta-decay calculations are analogous except for the difference in momentum transfer. As the momentum transferred to the nucleon in muon capture is of the order of 100 MeV/c, whereas beta decay involves a momentum of about 0.5 MeV/c, muon-capture rates are more sensitive to the momentum-transfer terms in the interaction Hamiltonian. Also in beta decay one can measure an energy spectrum as well as a transition rate, whereas in muon capture we can measure the transition rate only. The calculation of beta decay has been very successful, so we assume that the same techniques can be applied to muon-capture calculations after the momentum-dependent terms in the Hamiltonian have been included.

Several groups have calculated the muon-capture rate in O^{16}. The first calculations showed that the $0^+ \rightarrow 0^-$ transition rate is sensitive to the induced pseudoscalar coupling, but they neglected momentum corrections to the Hamiltonian and they did not include any admixtures in their nuclear wave functions.[1] A second calculation by Duck took these corrections into account and he calculated his own O^{16} wave functions.[16] However his O^{16} wave functions disagree with the more extensive analysis of Elliott and Flowers[17] and Gillet.[18] We have repeated these calculations using a different method and we have calculated the rates for several different cases. In order to test the simplifying assumptions of these earlier works, our calculations are done both with and without the small components of the relativistic muon-wave function for a point-charge nucleus. The uncertainty arising from the determination of the nuclear radius is also tested. These computations can then be compared with the experimental data presented in Sec. II.

B. Method for Calculating the Transition Rate

In calculating the muon-capture rates, we have used the method of Morita and Fujii.[19] They described the muon capture in terms analogous to beta decay by calculating the rate for various orders of forbiddenness. Also they avoid the use of simplifying assumptions, which can introduce additional uncertainties into the calculations.

Their analysis begins by using the Hamiltonian introduced by Weinberg[20]

$$\mathcal{H} = (\bar{\psi}_\nu \gamma_\lambda \psi_\ell)\bar{\psi}_n [C_V \gamma_\lambda - i C_M \sigma_{\lambda\mu} p_\mu + i C_S \frac{p_\lambda}{m_\mu}] \psi_p$$

$$+ (\bar{\psi}_\nu i \gamma_\lambda \gamma_5 \psi_\ell)\bar{\psi}_n [i C_A \gamma_\lambda \gamma_5 - C_P \frac{p_\lambda}{m_\mu} \gamma_5 - C_T \sigma_{\lambda\mu} \gamma_5 \frac{p_\mu}{W_0}] \psi_p \qquad (2)$$

where C_V is the vector-coupling constant given by beta decay, C_M is found by comparing the weak current with the electromagnetic current, C_S is an "induced scalar" coupling (which has not been observed), C_A is the axial-vector-coupling constant obtained from beta decay, C_P is the pseudoscalar coupling constant, C_T is the "induced tensor" coupling constant (which has not been observed), and W_0 is the energy difference between the initial and final nuclear states.

To calculate the matrix elements for the Hamiltonian, we need relativistic wave functions for the nucleus. Since only nonrelativistic nuclear wave functions are available, the nuclear-matrix elements must be calculated in a nonrelativistic approximation. This is done by means of a Foldy-Wouthuysen transformation to remove the odd operators from the Hamiltonian. The odd operators connect the upper and lower parts (positive- and negative-energy solutions) of the wave function. When these operators are removed, the matrix element can be found in terms of two component spinors, and a Hamiltonian is

derived that is good to order P/M (velocity of the nucleon). It should be noted that the transformation ignores mesic exchange currents in the nucleus,[21] but these processes do not seem to alter the nucleon properties in the nucleus.[22]

The lepton part of the interaction is treated relativistically by expanding the plane-wave neutrino in a spherical representation in terms of spinors with a definite angular momentum κ

$$\begin{aligned} \ell &= \kappa \qquad j = \ell - 1/2 \qquad \text{for} \quad \kappa > 0 \\ \ell &= -\kappa - 1 \qquad j = \ell + 1/2 \qquad \text{for} \quad \kappa < 0 \end{aligned}$$

and spin projection μ. The radial part of the neutrino-wave function is given by

$$\begin{aligned} g_\kappa &= \frac{1}{\sqrt{\pi}} \; j_\ell(qr) \\ f_\kappa &= \frac{1}{\sqrt{\pi}} \; S_\kappa \; j_{\bar{\ell}}(qr), \end{aligned} \tag{3}$$

where S_κ is the sign of κ, $j_\ell(qr)$ is a spherical Bessel function, ℓ is the orbital momentum corresponding to κ, and $\bar{\ell}$ is the orbital momentum corresponding to $-\kappa$. The muon wave function is treated in the same representation, but it has a simple form since the muon is assumed to be captured from the $1s_{1/2}$ orbit.

$$G_{-1} = \left(\frac{2Z}{a_0}\right)^{3/2} \left[\frac{1+\gamma}{2\Gamma(2\gamma+1)}\right]^{1/2} e^{-Zr/a_0} \left(\frac{2Zr}{a_0}\right)^{\gamma-1} \tag{4}$$

$$F_{-1} = -\left(\frac{1-\gamma}{1+\gamma}\right)^{1/2} G_{-1}, \qquad \text{where} \quad \gamma = \left[1-(\alpha Z)^2\right]^{1/2}$$

and F_{-1} is referred to as the small component of the muon wave function. These wave functions are for a point nucleus. The

calculation is easily adapted to a finite nucleus by means of the wave functions of Refs. 12 or 23, but the correction is probably unimportant compared to the other uncertainties in the problem. Flamand and Ford[22] found that the muon-capture rate in carbon was 6% less for a finite nucleus calculated relativistically than for a point nucleus calculated nonrelativistically. Ford believes that most of this correction was due to the relativistic effect and not to a finite size effect.[24]

The angular momenta (j) of the muon and neutrino are coupled to a total spin u, and the orbital angular momenta (ℓ) are coupled to a total spin v. In this representation, selection rules can be used for the nuclear transition. By conservation of angular momentum

$$|J_i - J_f| \leq u \leq |J_i + J_f| .$$

For O^{16}, $J_i = 0$, then $u = J_f$ and the lepton system has a definite spin.

The transition rate from the ground state $|0\rangle$ of spin J=0 to the excited state $|f\rangle$ of spin J_f and excitation energy W_0 ($W_0 = E_f - E_0$) is given by (using units $\hbar = c = m_e = 1$)

$$\lambda = 2\pi \left| \langle f | H | 0 \rangle \right|^2_{avg} q^2 \frac{dq}{dE} , \qquad (5)$$

where q is the momentum of the neutrino and dq/dE is a density-of-states factor,

$$\frac{dq}{dE} = 1 - \frac{q}{m_\mu + AM} . \qquad (6)$$

The expression $\langle f | H | 0 \rangle$ is given by Morita-Fujii in terms of the reduced nuclear-matrix elements $\mathcal{M}^{(i)}_{vu}(\kappa)$ and the coupling constants $C^{(i)}$

$$\left| \langle f | H | 0 \rangle \right|^2_{avg} = \frac{2J_f+1}{2} \sum_{i,j} \sum_{\kappa} C^{(i)} C^{(j)} \left[\sum_{v} \mathcal{M}^{(i)}_{vu}(\kappa) \right] \left[\sum_{v'} \mathcal{M}^{(j)}_{v'u}(\kappa) \right] \tag{7}$$

where

$$\mathcal{M}^{(i)}_{vu}(\kappa) = \frac{1}{\hat{J}_f} \langle f \| \Xi^{(i)} \| 0 \rangle \tag{8}$$

is a one-body matrix element (between states $|0\rangle$ and $|f\rangle$), which neglects phase factors common to all matrix elements. We use the notation $\hat{J}_f \equiv \sqrt{2J_f+1}$. The terms $\Xi^{(i)}$ are listed in Table V with the coupling constants $C^{(i)}$ as given by Morita-Fujii.[19] New entries in this table for the induced scalar (C_S) and induced tensor (C_T) couplings have been computed by Morita and Morita.[25] In our calculations we have used the following values for the coupling constants:

$$C_A^\beta = -1.18\, C_V^\beta$$

$$C_V = 0.972\, C_V^\beta$$

$$C_A = 0.999\, C_A^\beta$$

$$C_V^\beta = 1.015 \times 10^{-5}/M^2$$

$$C_M = \frac{3.706\, C_V}{2M}$$

$$C_S = 0$$

$$C_T = 0,$$

Where M is the proton mass.

Table V. Coupling constants $C^{(i)}$ and operators $\Xi^{(i)}$ in Eqs. (7) and (8). Subscript s refers to nuclear variables.

i	$C^{(i)}$	Ξ
1	C_V	$\mathscr{D}^{M_f-M_i}_{0vu}(\hat{r}_s)[g_\kappa G_{\kappa'} S_{0vu}(\kappa,\kappa') - f_\kappa F_{\kappa'} S_{0vu}(-\kappa,-\kappa')]\delta_{vu}$
2	$-C_A+C_T$	$\mathscr{D}^{M_f-M_i}_{1vu}(\hat{r}_s,\sigma_s)[g_\kappa G_{\kappa'} S_{1vu}(\kappa,\kappa') - f_\kappa F_{\kappa'} S_{1vu}(-\kappa,-\kappa')]$
3	$-C_V/M$	$i[f_\kappa G_{\kappa'} S_{1vu}(-\kappa,\kappa') + g_\kappa F_{\kappa'} S_{1vu}(\kappa,-\kappa')]\mathscr{D}^{M_f-M_i}_{1vu}(\hat{r}_s,p_s)$
4	$-\sqrt{3}C_V/2M$	$\{[(v+1)/(2v+3)]^{1/2}\mathscr{D}^{M_f-M_i}_{0\,v+1\,u}(\hat{r}_s)\delta_{v+1\,u}D_+ - [v/(2v-1)]^{1/2}\mathscr{D}^{M_f-M_i}_{0\,v-1\,u}(\hat{r}_s)\delta_{v-1\,u}D_-\}$ $\times [f_\kappa G_{\kappa'} S_{1vu}(-\kappa,\kappa') + g_\kappa F_{\kappa'} S_{1vu}(\kappa,-\kappa')]$
5	$-(\frac{3}{2})^{1/2}C_V(1+\mu_p-\mu_n)/M$	$[(v+1)^{1/2}W(1\,1uv,1v+1)\mathscr{D}^{M_f-M_i}_{1\,v+1\,u}(\hat{r}_s\sigma_s)D_+ - v^{1/2}W(1\,1uv,1v-1)\mathscr{D}^{M_f-M_i}_{1\,v-1\,u}(\hat{r}_s,\sigma_s)D_-]$ $\times [f_\kappa G_{\kappa'} S_{1vu}(-\kappa,\kappa') + g_\kappa F_{\kappa'} S_{1vu}(\kappa,-\kappa')]$
6	C_A/M	$i\mathscr{D}^{M_f-M_i}_{0vu}(\hat{r}_s)[f_\kappa G_{\kappa'} S_{0vu}(-\kappa,\kappa') + g_\kappa F_{\kappa'} S_{0vu}(\kappa,-\kappa')]\sigma_s\cdot p_s$
7	$-\frac{1}{\sqrt{3}}\left[\frac{C_A}{2M} - \frac{C_T}{W_0}\right]$	$\{[(v+1)/(2v+1)]^{1/2}\mathscr{D}^{M_f-M_i}_{1\,v+1\,u}(\hat{r}_s,\sigma_s)D_+ - [v/(2v+1)]^{1/2}\mathscr{D}^{M_f-M_i}_{1\,v-1\,u}(\hat{r}_s,\sigma_s)D_-\}$
8	$C_P/2\sqrt{3}M$	$\times [f_\kappa G_{\kappa'} S_{0vu}(-\kappa,\kappa') \pm g_\kappa F_{\kappa'} S_{0vu}(\kappa,-\kappa')]\delta_{vu}$
9	C_S	$\mathscr{D}^{M_f-M_i}_{0vu}(\hat{r}_s)[g_\kappa G_{\kappa'} S_{0vu}(\kappa,\kappa') + f_\kappa F_{\kappa'} S_{0vu}(-\kappa,-\kappa')]\delta_{vu}$

The term C_P is treated as a free parameter. If the vector and axial-vector currents behave properly under G conjugation, C_S and C_T are equal to zero. With our limited amount of data, we must make this assumption to simplify the calculation of C_P.

The nuclear integration gives (we use the phases of Edmonds[26])

$$\left.\begin{matrix}\langle A||\Xi^{(1)}||a\rangle \\ \langle A||\Xi^{(9)}||a\rangle\end{matrix}\right\} = \langle \ell_A||\mathcal{D}_{0vu}(\hat{r})||\ell_a\rangle \times \int_0^\infty u_A\left[g_\kappa G_{\kappa'} S_{0vu}(\kappa,\kappa') \mp f_\kappa F_{\kappa'} S_{0vu}(-\kappa,-\kappa')\right] u_a r^2 dr$$

where the - sign refers to i=1 and the + sign to i=9.

$$\langle A||\Xi^{(2)}||a\rangle = \langle \ell_A||\mathcal{D}_{1vu}(\hat{r},\vec{\sigma})||\ell_a\rangle \times \int_0^\infty u_A\left[g_\kappa G_{\kappa'} S_{1vu}(\kappa,\kappa') - f_\kappa F_{\kappa'} S_{1vu}(-\kappa,-\kappa')\right] u_a r^2 dr.$$

$$\langle A||\Xi^{(3)}||a\rangle = (-)^{3/2+j_a+\ell_a+\ell_A+v-u} \frac{\sqrt{3}}{4\pi} \hat{j}_A \hat{j}_a \hat{u} \hat{\ell}_A \hat{v} \begin{Bmatrix} \ell_A & j_A & 1/2 \\ j_a & \ell_a & u \end{Bmatrix} \times \sum_{\ell'=\ell_a\pm1} \hat{\ell'} \begin{Bmatrix} v & 1 & u \\ \ell_a & \ell_A & \ell' \end{Bmatrix} \begin{pmatrix} \ell_A & v & \ell' \\ 0 & 0 & 0 \end{pmatrix} \times \int u_A\left[f_\kappa G_{\kappa'} S_{1vu}(-\kappa,\kappa') + g_\kappa F_{\kappa'} S_{1vu}(\kappa,-\kappa')\right] D_{\ell'} u_a r^2 dr,$$

where

$$D_{\ell'} = \frac{(-)^{\ell_a}\sqrt{3}(\ell_a+1)\left(\frac{d}{dr} - \frac{\ell_a}{r}\right)}{\left[(2\ell_a+1)(2\ell_a+3)\right]^{1/2}(\ell' \ \ell_a \ \ 00|10)} \qquad \text{if } \ell' = \ell_a + 1,$$

and

$$D_{\ell'} = \frac{(-)^{\ell_a}\sqrt{3}\,\ell_a\left(\frac{d}{dr} + \frac{\ell_a+1}{r}\right)}{\left[(2\ell_a-1)(2\ell_a+1)\right]^{1/2}(\ell' \ \ell_a \ \ 00|10)} \qquad \text{if } \ell' = \ell_a - 1$$

are operators that act on u_a.

$$\langle A||\Xi^{(4)}||a\rangle = \left(\frac{v+1}{2v+3}\right)^{1/2} \langle \ell_A||\mathcal{Y}_{0\,v+1\,u}(\hat{r})||\ell_a\rangle \ \delta_{v+1,u}$$

$$\times \int_0^\infty u_A D_+ \left[f_\kappa G_{\kappa'} S_{1vu}(-\kappa,\kappa') + g_\kappa F_{\kappa'} S_{1vu}(\kappa,-\kappa')\right] u_a r^2 dr$$

$$-\left(\frac{v}{2v-1}\right)^{1/2} \langle \ell_A||\mathcal{Y}_{0\,v-1\,u}(\hat{r})||\ell_a\rangle \ \delta_{v-1,u}$$

$$\times \int_0^\infty u_A D_- \left[f_\kappa G_{\kappa'} S_{1vu}(-\kappa,\kappa') + g_\kappa F_{\kappa'} S_{1vu}(\kappa,-\kappa')\right] u_a r^2 dr$$

where $D_+ = \frac{d}{dr} - \frac{v}{r}$ and $D_- = \frac{d}{dr} + \frac{v+1}{r}$ are operators that act only on the lepton wave functions.

$$\langle A||\Xi^{(5)}||a\rangle = (v+1)^{1/2}\, W(11uv,\ 1\,v+1)\, \langle \ell_A||\mathscr{D}_{1\,v+1\,u}(\hat{r},\vec{\sigma})||\ell_a\rangle$$

$$\times\int_0^\infty u_A D_+ \left[f_\kappa G_{\kappa'}\, S_{1vu}(-\kappa,\kappa') + g_\kappa F_{\kappa'}\, S_{1vu}(\kappa,-\kappa') \right] u_a r^2 dr$$

$$- v^{1/2}\, W(11uv,\ 1\,v-1)\, \langle \ell_A||\mathscr{D}_{1\,v-1\,u}(\hat{r},\vec{\sigma})||\ell_a\rangle$$

$$\times\int_0^\infty u_A D_- \left[f_\kappa G_{\kappa'}\, S_{1vu}(-\kappa,\kappa') + g_\kappa F_{\kappa'}\, S_{1vu}(\kappa,-\kappa') \right] u_a r^2 dr$$

$$\langle A||\Xi^{(6)}||a\rangle =$$

$$(-)^{\ell_a+j_a+1/2}\sqrt{6} \sum_{\ell'=\ell_a\pm1} \langle \ell_A||\mathscr{D}_{0vu}(\hat{r})||\ell'\rangle \begin{Bmatrix} j_a & 1/2 & \ell' \\ 1 & \ell_a & 1/2 \end{Bmatrix}$$

$$\times\int_0^\infty u_A \left[f_\kappa G_{\kappa'}\, S_{0vu}(-\kappa,\kappa') + g_\kappa F_{\kappa'}\, S_{0vu}(\kappa,-\kappa') \right] D_{\ell'}\, u_a r^2\, dr$$

$$\left.\begin{matrix} \langle A||\Xi^{(7)}||a\rangle \\ \langle A||\Xi^{(8)}||a\rangle \end{matrix}\right\} = \left(\frac{v+1}{2v+1}\right)^{1/2} \langle \ell_A||\mathscr{D}_{1\,v+1\,u}(\hat{r},\vec{\sigma})||\ell_a\rangle\ \delta_{vu}$$

$$\times\int_0^\infty u_A D_+ \left[f_\kappa G_{\kappa'}\, S_{0vu}(-\kappa,\kappa') \pm g_\kappa F_{\kappa'}\, S_{0vu}(\kappa,-\kappa') \right] u_a r^2 dr$$

$$- \left(\frac{v}{2v+1}\right)^{1/2} \langle \ell_A||\mathscr{D}_{1\,v-1\,u}(\hat{r},\vec{\sigma})||\ell_a\rangle\ \delta_{vu}$$

$$\times\int_0^\infty u_A D_- \left[f_\kappa G_{\kappa'}\, S_{0vu}(-\kappa,\kappa') \pm g_\kappa F_{\kappa'}\, S_{0vu}(\kappa,-\kappa') \right] u_a r^2 dr,$$

where the + sign refers to i=7 and the - sign to i=8. The symbols A and a indicate the ℓsj quantum numbers for the respective state. Here u_A and u_a are harmonic oscillator wave functions,

$$u_{n,\ell}(r) = N\, b^{-\ell-3/2}\, P(r) r^{\ell}\, e^{-1/2(r/b)^2}$$

where N is a normalization constant

$$N = \frac{1}{\pi^{1/4}} \sqrt{\frac{2^{n+\ell+1}}{(2n+2\ell-1)!!}} ,$$

b is the oscillator length parameter, and

$$P(r) = 1 \qquad \text{for } n = 1$$

$$= \frac{2\ell+1}{2} - \left(\frac{r}{b}\right)^2 \qquad \text{for } n = 2$$

$$= \frac{1}{2}\left[\frac{(2\ell+3)(2\ell+5)}{4} - (2\ell+5)\left(\frac{r}{b}\right)^2 + \left(\frac{r}{b}\right)^4\right] \qquad \text{for } n = 3.$$

We use the following reduced matrix elements

$$\langle \ell_A \| \mathcal{Y}_{0vu}(\hat{r}) \| \ell_a \rangle = \frac{(-)^{1/2+j_a+u}}{4\pi}\, \hat{j}_a \hat{j}_A \hat{\ell}_A \hat{\ell}_a \hat{u} \begin{Bmatrix} \ell_A & j_A & 1/2 \\ j_a & \ell_a & u \end{Bmatrix} \begin{pmatrix} \ell_A & u & \ell_a \\ 0 & 0 & 0 \end{pmatrix}$$

$$\langle \ell_A \| \mathcal{Y}_{1vu}(\hat{r},\vec{\sigma}) \| \ell_a \rangle = (-)^{1+v+\ell_A-u} \frac{3}{\sqrt{8\pi}}\, \hat{\ell}_A \hat{\ell}_a \hat{v} \hat{j}_a \hat{j}_A \hat{u}$$

$$\times \begin{pmatrix} \ell_A & v & \ell_a \\ 0 & 0 & 0 \end{pmatrix} \begin{Bmatrix} \ell_A & \ell_a & v \\ 1/2 & 1/2 & 1 \\ j_A & j_a & u \end{Bmatrix}$$

$$S_{kvu}(\kappa,\kappa') = \sqrt{2}\, \hat{\ell}\hat{\ell}'\, \hat{j}\hat{j}'\, (\ell\ell'\ 00|v0) \begin{Bmatrix} \ell & \ell' & v \\ j & j' & u \\ 1/2 & 1/2 & k \end{Bmatrix} .$$

C. Nuclear Wave Functions

A calculation of C_p requires a good knowledge of the nuclear wave function. The purpose of the present work is to determine the uncertainty in the computation of C_p due to uncertainties of the nuclear wave functions coming from

(a) lack of knowledge of the parameters in the potential,

(b) uncertain nuclear-well parameters,

(c) the nuclear problem itself, which is only approximately solved.

Three nuclear models are used:

(a) the independent-particle model (IP),

(b) the diagonalization of the residual interaction in the subspace of $1\hbar\omega$ particle-hole excitations (approximation I),

(c) the random phase approximation (approximation II).

The nuclear matrix elements in the particle-hole model are

$$\langle f|H|0\rangle = \sum_{Aa} X'_{Aa} \langle A|H|a\rangle + Y'_{Aa} \langle a|H|A\rangle \qquad (9)$$

where $\langle A|H|a\rangle$ is a one body matrix element between the hole state a and the particle state A, and the X'_{Aa} (Y'_{Aa}) is the probability amplitude for exciting the nuclear state $|f\rangle$ by creation (destruction) of a particle-hole pair $|Aa\rangle$ in the ground state.

We have used the particle-hole phases of Bell[27] in the probability amplitudes X and Y in computing the reduced matrix elements $\mathcal{M}^{(i)}_{vu}$. The probability amplitudes X' and Y' for the particle-hole pairs as tabulated by Gillet must be multiplied by a phase factor

$$X_{Aa} = (-1)^{j_a+1/2} X'_{Aa}$$

$$Y_{Aa} = (-1)^{j_A+1/2} Y'_{Aa} \qquad (10)$$

Then the reduced matrix elements are given by

$$\langle f||\Xi^{(i)}||0\rangle = \sum_{Aa} X_{Aa} \langle A||\Xi^{(i)}||a\rangle + Y_{Aa} \langle a||\Xi^{(i)}||A\rangle . \quad (11)$$

In the independent-particle model (IP) one X_{Aa} is equal to 1, the other X_{Aa} and Y_{Aa} terms are equal to zero. In approximation I:

$$X_{Aa} \neq 0, \quad Y_{Aa} = 0, \quad \text{and} \quad \sum_{Aa} |X_{Aa}|^2 = 1.$$

In approximation II,

$$X_{Aa} \neq 0, \quad Y_{Aa} \neq 0, \quad \text{and} \quad \sum_{Aa} |X_{Aa}|^2 - |Y_{Aa}|^2 = 1.$$

In approximation I we use wave functions derived from two different potentials. The first potential is the Rosenfeld mixture used by Elliott and Flowers,[17] and the second potential is found from a least-squares search carried over nine energy levels of O^{16} by Gillet.[18] Wave functions are derived from the potentials by finding the set of basis vectors ψ_α for which the matrix $\langle \psi_\alpha | V | \psi_\beta \rangle$ is diagonal. Since two values of the potential V were used in these two analyses, two different wave functions are obtained. Both potentials, with strongly different characteristics as seen from Table VI, give similar overall good fits for the energies. However, the different potentials affect the small components of the nuclear wave function appreciably, as shown in Table VII, allowing a numerical discussion of the uncertainties due to the nuclear paramters. It should be noted that Elliott and Flowers use a phase convention that is different from Gillet's convention. The differences are:

(a) They use a slj coupling order in their work whereas Gillet uses a lsj order. This introduces a relative phase of $(-)^{j_a + j_A}$.

(b) They use a different phase convention for their 2s harmonic oscillator function which introduces a relative minus sign for all of the 2s amplitudes.

(c) Gillet introduces a phase factor $(-)^{j_A+1/2}$ to symmetrize a matrix.

The phases in Table VII have been corrected to Gillet's convention.

The wave function for the two potentials are much different. This could indicate that either the wave function is very sensitive to the nuclear model, or we have not included all of the phase factor differences between these two works.

Table VI. Nuclear potential used in calculating O^{16} wave functions.[a,b]

	V(MeV)	μ/b	H	θ	η
Elliott and Flowers[a]	-40	0.90	-0.26	1.06	0.6
Gillet[c]	-40	1.0	0.4	0	0.4

[a]Ref. 17.

[b]In this table the potential is defined by

$$V(r) = f(r/\mu)V(W + BP_\sigma - HP_\gamma + MP_\sigma P_\gamma)$$

P_σ and P_γ are spin and isobaric-spin exchange operators, $f(r/\mu)$ is a radial form factor, V is the potential depth, W, B, H, and M are the four exchange coefficients, b is the oscillator-length parameter, and μ is the range of the force.

$$\theta = M - W$$

$$\eta = M + W - B - H$$

[c]Ref. 18.

Table VII. The wave function amplitudes X' and Y' for O^{16} as given by the particle-hole models. The phases of the Elliott and Flower wave functions are modified, relative to their work, to be consistent with the convention used by Gillet in finding I_G. In the case of approximation II, the X' and Y' amplitudes are given in that order. These amplitudes must be multiplied by a phase factor as shown in Eq. (10).

N^{16}		$1p_{-1/2}$	$1p_{-1/2}$	$1p_{-1/2}$	$1p_{-3/2}$	$1p_{-3/2}$	$1p_{-3/2}$	$2s_{-1/2}$	$1d_{-5/2}$	$1d_{-3/2}$	$2s_{-1/2}$	$1d_{-5/2}$	$1d_{-3/2}$
State	Model	$2s_{1/2}$	$1d_{5/2}$	$1d_{3/2}$	$2s_{1/2}$	$1d_{5/2}$	$1d_{3/2}$	$1p_{1/2}$	$1p_{1/2}$	$1p_{1/2}$	$1p_{3/2}$	$1p_{3/2}$	$1p_{3/2}$
	IP	1.00	-	-	-	-	-	-	-	-	-	-	-
0^-	I_{EF}	1.00	-	-	-	-	0.05	-	-	-	-	-	-
	I_G	0.999	-	-	-	-	-0.055	-	-	-	-	-	-
	II	0.999	-	-	-	-	-0.053	-0.012	-	-	-	-	-0.012
	IP	1.00	-	-	-	-	-	-	-	-	-	-	-
1^-	I_{EF}	0.98	-	0.01	0.16	0.08	0.02	-	-	-	-	-	-
	I_G	0.995	-	-0.008	-0.026	0.096	0.020	-	-	-	-	-	-
	II	0.996	-	-0.006	-0.026	0.090	0.019	0.001	-	-0.009	0.012	0.008	-0.008
	IP	-	1.00	-	-	-	-	-	-	-	-	-	-
2^-	I_{EF}	-	0.98	-0.10	-0.06	-0.14	-0.09	-	-	-	-	-	-
	I_G	-	0.983	0.007	-0.054	-0.174	-0.035	-	-	-	-	-	-
	II	-	0.985	0.007	-0.051	-0.166	-0.034	-	-0.026	-0.001	-0.009	-0.020	-0.015
	IP	-	1.00	-	-	-	-	-	-	-	-	-	-
3^-	I_{EF}	-	0.98	-	-	0.18	-0.06	-	-	-	-	-	-
	I_G	-	0.998	-	-	0.062	0.011	-	-	-	-	-	-
	II	-	0.999	-	-	0.059	0.010	-	0.000	-	-	0.004	-0.029

D. Results

The reduced matrix elements $\mathcal{M}_{vu}^{(i)}$ were calculated on an IBM-7094 computer to allow the use of numerical methods to evaluate the radial integrals. In checking our method, we first calculated the muon-capture rate in C^{12} to the ground state of B^{12}. Because of ambiguities in the nuclear wave function, the computed capture rate does not agree with the rate determined experimentally. Morita and Fujii[19] correct this by taking a ratio with the inverse-beta-decay transition, and obtain for the capture rate

$$\lambda_{exp}^{\mu} = \frac{\lambda_{calc}^{\mu}}{\lambda_{calc}^{\beta}} \lambda_{exp}^{\beta} , \qquad (12)$$

where λ_{calc}^{μ} is the muon-capture rate calculated with the Morita-Fujii method, and λ_{exp}^{μ} is the observed rate. Using[19]

$$\lambda_{exp}^{\beta} = 33.15 \text{ sec}^{-1} \text{ and}$$

$$\lambda_{calc}^{\beta} = 159 \text{ sec}^{-1},$$

we obtain the results given in Table VIII. Figure 12 shows λ_{exp}^{μ} as a function of C_P/C_A and the experimental value of 6750^{+300}_{-750} sec^{-1} measured by Maier et al.[28] From the graph we would conclude $10 < C_P/C_A < 30$, where we have not allowed for errors in the nuclear wave function. The capture rate λ_{calc}^{μ} has been computed by Morita with his method where he has set the small components of the muon-wave function equal to zero. For the same case, we obtain a transition rate of 35.0×10^3 sec^{-1}, which compares with the value 34.2×10^3 sec^{-1}, that Morita and Fujii compute. This good agreement provides a check on our computer program.

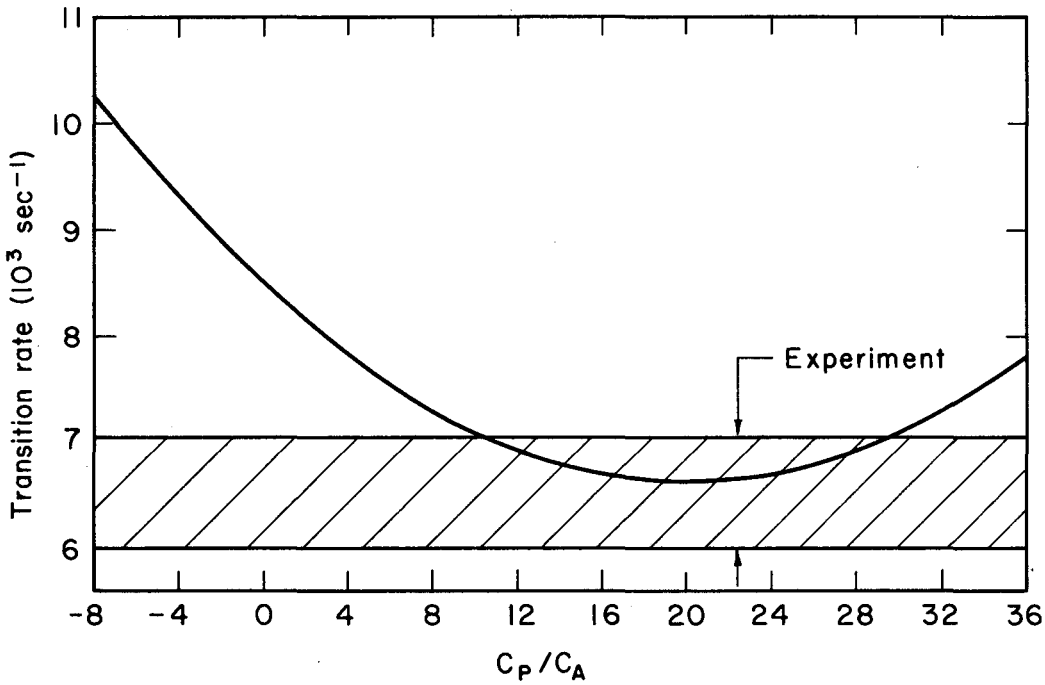

Fig. 12. Muon-capture rate in C^{12}.

Table VIII. Capture rate in C^{12} leading to the $J^P = 1^+$ ground state of B^{12}. The terms λ^{μ}_{calc} and λ^{μ}_{exp} are defined in Eq. (12). We use b = 1.59 f.

C_P/C_A	λ^{μ}_{calc}	λ^{μ}_{exp}
-8	49.5	10.3
-4	44.8	9.33
0	40.8	8.50
4	37.5	7.81
8	35.0	7.29
12	33.2	6.92
16	32.1	6.69
20	31.7	6.60
24	32.1	6.69
28	33.1	6.90
32	35.0	7.29
36	37.5	7.81

In Table IX we compare the theoretical transition rates, using the wave functions I_G of Table VII with and without the small relativistic component of the muon wave function. This component has been neglected in earlier calculations. Neglect of the small component increases the 0^- transition rate and decreases the 1^-, and 3^- transition rates. The small component affects the transition rate by only a few percent, which is insignificant when compared with the other sources of uncertainty discussed in the following sections. Nevertheless, the small component is included in the following results.

The oscillator-length parameter b that enters into the oscillator-well-wave functions is, in principle, given by an analysis of the elastic electron-scattering data, i.e., 1.75 f for O^{16}.[29] In Table X we show the results of varying the O^{16} oscillator length by 15% while using the wave functions of case I_G. A 15% change in b produces a 10 to 15% change in the 0^- transition rate for $C_P/C_A \approx 7$.

Table IX. Effect of neglecting the small relativistic component of the bound-muon wave function. Column 2 is obtained by using the complete wave function and column 1 is obtained by using only the large component of the wave function in Eq. (4). The nuclear wave function used is the case I_G, Table III.

C_P/C_A	Transition rate (10^3 sec^{-1})							
	0^-		1^-		2^-		3^-	
	1	2	1	2	1	2	1	2
-8	4.80	4.73	2.54	2.53	25.7	25.8	0.186	0.196
-4	3.88	3.83			22.6	22.7		
0	3.06	3.01			20.0	20.0		
4	2.33	2.30			17.8	17.8		
8	1.71	1.68			16.0	16.0		
12	1.18	1.16			14.6	14.6		
16	0.749	0.735			13.8	13.7		
20	0.415	0.406			13.3	13.2		
24	0.179	0.174			13.3	13.2		
28	0.0411	0.0392			13.7	13.6		
32	0	0			14.6	14.4		
36	0.0571	0.0584			15.9	15.7		

Table X. Effect of the variation of the oscillator-length parameter. Columns 1, 2, and 3 correspond to $1/b = 0.51$, 0.57, and $0.63\ f^{-1}$, respectively. The central value is the one obtained from elastic-electron-scattering data. The wave functions used are the ones of case I_G of Table IV.

C_P/C_A	Transition rate (10^3 sec^{-1})											
	0^-			1^-			2^-			3^-		
	1	2	3	1	2	3	1	2	3	1	2	3
-8	4.30	4.73	5.03	2.48	2.53	2.45	27.8	25.8	23.6	0.343	0.196	0.116
-4	3.46	3.83	4.09				24.5	22.7	20.7			
0	2.71	3.01	3.25				21.7	20.0	18.2			
4	2.05	2.30	2.50				19.4	17.8	16.1			
8	1.49	1.68	1.85				17.5	16.0	14.4			
12	1.01	1.16	1.30				16.1	14.6	13.1			
16	0.627	0.735	0.849				15.1	13.7	12.2			
20	0.334	0.406	0.491				14.6	13.2	11.8			
24	0.133	0.174	0.231				14.6	13.2	11.8			
28	0.0226	0.0392	0.0679				15.0	13.6	12.2			
32	0	0	0				15.9	14.4	12.9			
36	0.0768	0.0584	0.0323				17.2	15.7	14.1			

The transition rates for different nuclear models and b = 1.75 f are tabulated in Table XI. As one would expect for the almost pure states considered here, the transition computed with approximation II (RPA) and approximation I_G differ only slightly as shown in columns I_G and II. However the agreement in the transition rates for the I_{EF} and I_G wave functions is surprising because the small components of these wave functions are so different. Apparently the transition rate is not sensitive to the potential for the 1^-, 2^-, and 3^- transitions.

To test the dependence of the 0^- transition rate on the amplitude of the small component, we have computed the transition rate with the following wave functions

$$\psi_{IP} = |1\, p^{-1}_{1/2}\, 2\, s_{1/2}\rangle$$

$$\psi_A = 0.99\, |1p^{-1}_{1/2}\, 2\, s_{1/2}\rangle - 0.05\, |1\, p^{-1}_{3/2}\, 1\, d_{3/2}\rangle$$

$$\psi_B = 0.99\, |1p^{-1}_{1/2}\, 2\, s_{1/2}\rangle + 0.05\, |1\, p^{-1}_{3/2}\, 1\, d_{3/2}\rangle\,,$$

where ψ_A is the wave function computed in approximation I_G and we have changed the sign of the small component to obtain ψ_B. As shown in Fig. 13, large differences in the transition rates are associated with variations of the small component in the nuclear wave function. The sensitivity of the transition rates to the small component is to be expected since the small amplitude multiplies large one-body matrix elements in Eq. (11). Furthermore, the sensitivity is enhanced by the cross terms between large and small components in the expression for the transition rates of Eqs. (5) and (7).

Although the 3^- transition is third forbidden, its rate is 5% of the 1^- case, which is first forbidden. The high-momentum transfer in muon capture makes the forbidden transitions more important than in beta decay for which the comparable forbidden transitions would be negligible.

Table XI. Transition rates for different nuclear models.
See Table III for nuclear wave functions.

C_P/C_A	Transition rate (10^3 sec^{-1})							
	0^-				1^-			
	IP	I_{EF}	I_G	II	IP	I_{EF}	I_G	II
-8	6.45	8.09	4.73	4.81				
-4	5.18	6.46	3.83	3.91	4.69	4.25	2.53	2.36
0	4.04	5.01	3.01	3.10				
4	3.04	3.74	2.30	2.38				
8	2.19	2.66	1.68	1.76				
12	1.47	1.76	1.16	1.23				
16	0.900	1.05	0.735	0.795				
20	0.467	0.521	0.406	0.455				
24	0.175	0.175	0.174	0.209				
28	0.0234	0.0134	0.0392	0.0577				
32	0.0126	0.0352	0	0				
36	0.142	0.241	0.0584	0.0377				
	2^-				3^-			
-8	39.8	32.2	25.8	22.7				
-4	35.0	28.3	22.7	20.0				
0	30.9	24.9	20.0	17.6				
4	27.6	22.0	17.8	15.6	0.187	0.163	0.196	0.182
8	25.0	19.8	16.0	14.1				
12	23.1	18.1	14.6	12.9				
16	21.9	16.9	13.7	12.0				
20	21.5	16.3	13.2	11.6				
24	21.8	16.3	13.2	11.6				
28	22.8	16.9	13.6	11.9				
32	24.5	18.0	14.4	12.6				
36	27.0	19.7	15.7	13.8				

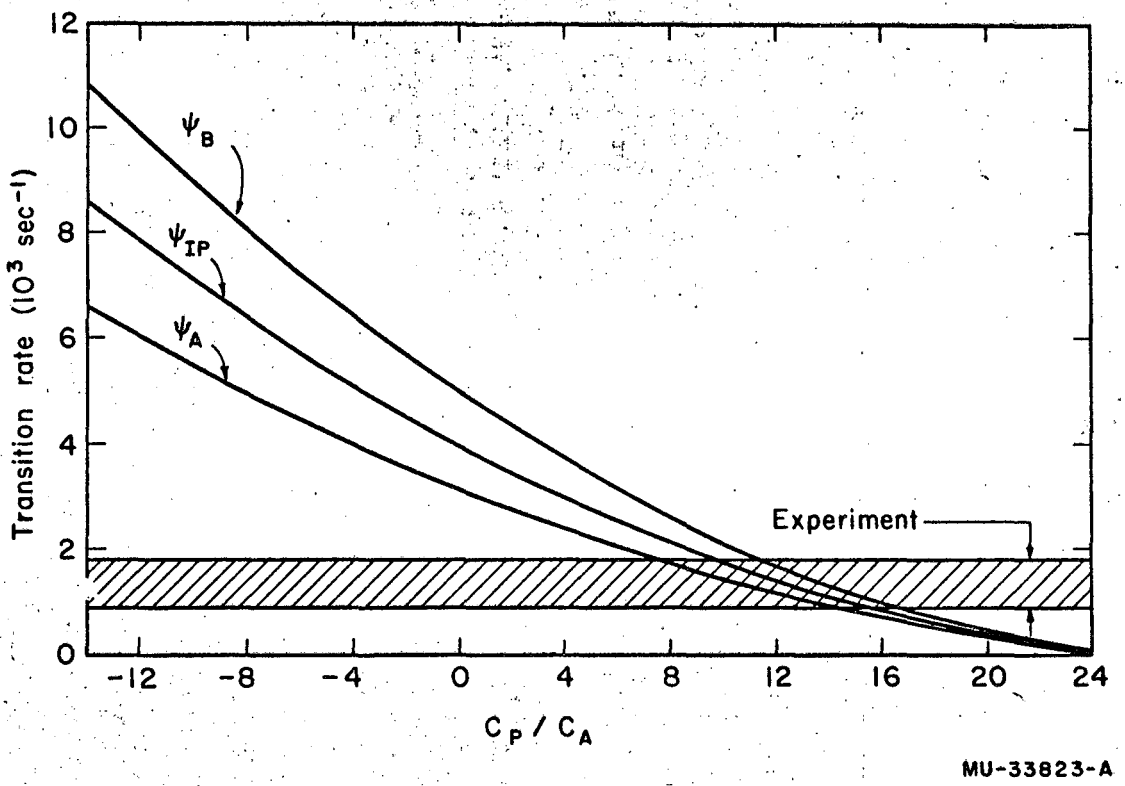

Fig. 13. Dependence of C_P on the small component of the nuclear wave function for muon capture in O^{16}. The experimental error includes both the Columbia data and the present measurement as given in Table IV.

E. Comparison with Earlier Work

It is interesting to look at the earlier works and compare them with our results. Beltrametti and Radicati have computed the matrix elements for capture in O^{16}, but they do not present the transition rates.[30] Duck does not present his rates for the $0^+ \rightarrow 0^-$ transition, but he computes $0^-/1^-$, the ratio of the $0^+ \rightarrow 0^-$ transition to the $0^+ \rightarrow 1^-$ transition.[16] Also, he computes the transition into the 2^- ground state. It is difficult to compute the $0^+ \rightarrow 0^-$ transition from data given in Duck's paper since there are disagreements in sign in the two publications of his work, e.g., see the phases of the wave functions and definitions of the coupling constants given in these two references. However, we can compare calculations by computing the $0^-/1^-$ ratio and the 2^- rate, using the Morita-Fujii method. This comparison is given in Table XII. Our results are different from those of Duck. We have used a different method, and we do not understand the reason for the discrepancy. It could be due to wrong phase factors in the nuclear wave function and the wrong handling of the lepton problem. A group at CERN has repeated these calculations independently and a preliminary report shows agreement with our 0^- calculation.[31]

Table XII. Comparison of transition rates computed for the same case with oscillator length b = 1.56 f and with the Elliott and Flower wave functions. The muon wave function is set equal to an average value in the radial integral and F, the small component of the muon wave function, equals zero.

C_P/C_A =	$0^-/1^-$			$2^-(10^3\ \text{sec}^{-1})^a$		
	-8	0	+8	-8	0	+8
Duck[b]	1.8	1.4	0.66	25.9	19.9	15.9
Present work	2.6	1.6	0.94	25.9	20.0	16.0

a. These rates have been computed with the muon wave function set equal to its value at the origin.

b. Reference 16, Tables 4b and 4c.

F. Analysis of Calculations

The results of our analysis can be summarized as follows:

(a) The capture rates into the 1^- and 3^- states are independent of C_P.

(b) Neglect of the small relativistic component of the muon wave function is consistent with the other sources of uncertainty in the problem.

(c) Large variations in the transition rates result from variations of the small components of the nuclear wave function, i.e., the determination of C_P/C_A is sensitive to the unknown two-body nuclear forces.

(d) A measurement of the $0^+ \rightarrow 0^-$ transition rate in O^{16} does not determine C_P uniquely. Figure 14 shows the transition rate as a function of C_P for nuclear model I_G, and there are two possible values of C_P for the given experimental value. Using the C^{12} data given in Fig. 12, we see that the higher value can be excluded.

(e) We conclude from the present analysis of the experimental data for muon capture in O^{16} that $5 < C_P/C_A < 20$ as seen in Fig. 13, which compares the theoretical rates we computed with the experimental rates of Sec. II. This agrees with the theoretical value of $C_P/C_A \approx 7$ predicted by Goldberger and Treiman.[2] The results are valid only if the induced pseudotensor term C_T is zero because the introduction of another unknown, C_T, would lead to more doubtful conclusions in the present state of the experimental evidence and of the nuclear model.

(f) The disagreement between theory and experiment for capture into the 1^- and 2^- states can probably be attributed to the many admixtures present in the wave functions. As shown for the 0^- rate, which has only one small component, transition rates are very sensitive to the small admixtures.

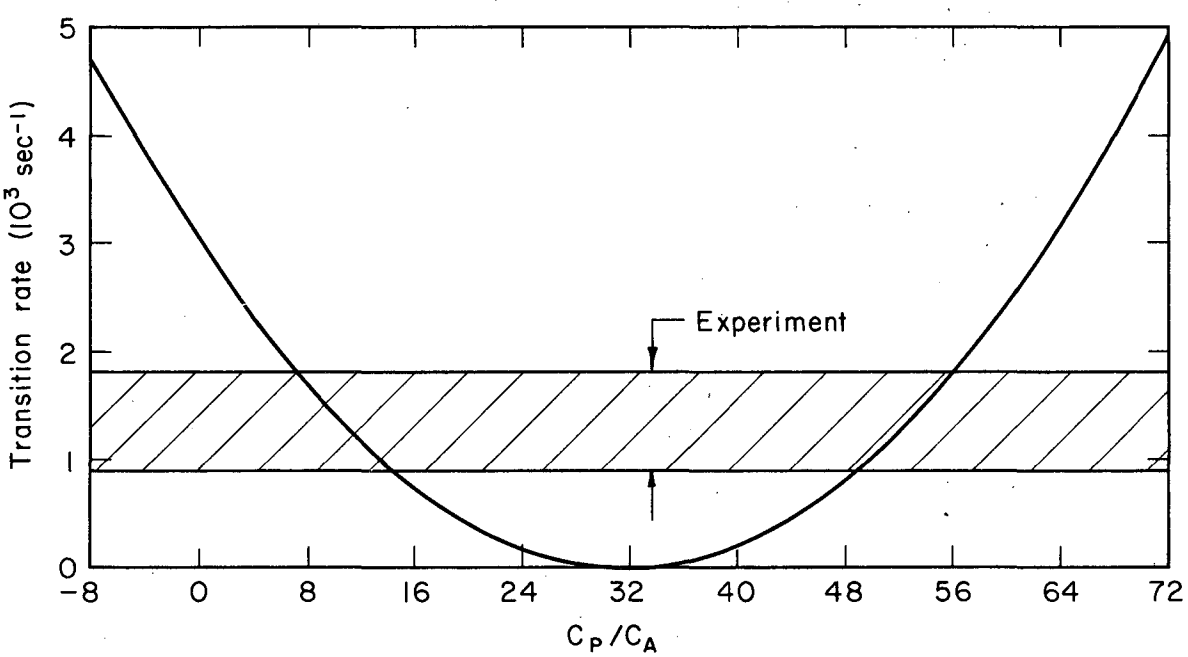

Fig. 14. Muon-capture rate in O^{16}.

IV. CONCLUSIONS

We have measured the muon-capture rate in oxygen to the 0^- state of N^{16}. Unfortunately the rate does not give a precise value of the pseudoscalar coupling constant because of the uncertainties in the nuclear wave function and the muon interaction. Several things can be done to improve the situation. First, an accurate nuclear wave function must be found for N^{16}. Cabibbo has suggested[32] that the amplitude for the small components could be found by using the wave functions to compute the electromagnetic transitions in N^{16}. With an accurate wave function, the coupling constant should be easy to find from this transition rate. Next, there is the question of the induced pseudotensor and pseudoscalar coupling constants. At present there are not enough experimental data to justify a search for these terms, and we must assume that they are zero to simplify the calculations. However, if they are present they could seriously affect the calculation of muon-capture rates. Thus far, the calculations for muon-capture rates have used a free parameter C_P and the other possible parameters C_S and C_T have been neglected. The absence of these terms could be ascertained by observing muon-capture transitions in which their matrix elements would be large compared to other terms in the Hamiltonian. For instance, a $0^+ \rightarrow 0^+$ transition would be useful for finding the C_S term because the axial-vector part of the Hamiltonian cannot contribute to the transition.

In gathering more experimental data, one must be careful to measure the muon-capture rates in those nuclei with wave functions that are reasonably well known. For this reason, the transitions $Mg^{24} \rightarrow Na^{24*}$ and $Ti^{48} \rightarrow Sc^{48*}$ have been suggested by Rasmussen.[33] Using the Nilsson model, Mang[34] has developed wave functions for Mg^{24}; and McCullen et al.[35] have published wave functions for Ti^{48}. At present the $Mg^{24} \rightarrow Na^{24}$ transition looks most promising because the excited states in Na^{24} are well known and these states must be known before an experiment can be planned to measure the transition

rate. The $Ti^{48} \rightarrow Sc^{48}$ transition is experimentally difficult at the moment because of the uncertainty in the excited states of Sc^{48}. There has been very little experimental investigation of Sc^{48} even though the energy levels have been predicted by McCullen et al.[35] and the spins of the levels have been predicted by Rasmussen.[33] If the highest excited states of Sc^{48} have $J^P = 0^+$ and 1^+ as indicated by Rasmussen, this nucleus may be useful for a muon-capture experiment.

Besides inquiring about the presence of various coupling constants, there are other questions that can be raised. Is the universal Fermi interaction valid? Are the coupling constants C_A and C_V the same for all nuclei? And when these questions have been answered, muon-capture rates may be useful in the study of nuclear structure since the rates are very sensitive to the nuclear wave function.

ACKNOWLEDGMENTS

I thank Professor Emilio Segrè for his support and encouragement during my graduate study in physics. I also thank Dr. Alan Astbury, Dr. Leonard B. Auerbach, David Cutts, Dr. Robert J. Esterling, Brian T. Guilbert, Dr. Norman H. Lipman, and Robert E. Shafer for their assistance in the capture-rate measurements and James Vale and the 184-inch cyclotron crew for their help. In addition, I thank Dr. Vincent Gillet for his aid and guidance during the shell-model calculations, Dr. M. Morita for explaining his paper and assisting in checking our calculations, and Dr. Torlief Ericson for informing us of his results.

The National Science Foundation was very kind in providing financial assistance for three years of my graduate study.

This work was done under the auspices of the U. S. Atomic Energy Commission.

APPENDICES

A. Background Analysis

1. Background Subtraction

To subtract the background in the pulse-height spectrum, we assume that the number of counts/channel in a time bin N_i can be written

$$N_i = \alpha_i N_{120} + \beta_i N_\mu + N_r,$$

where

N_{120} = total number of 120-keV gamma rays detected in NaI for all time,

α_i = fraction of N_{120} expected in the time bin τ_i,

N_μ = total number of target-derived pulses detected in NaI for all time,

β_i = fraction of N_μ expected in the time bin τ_i, and

N_r = total random counts in time bin τ_i.

The terms α_i and β_i are derived below.

Taking three time bins, we get three equations

$$N_1 = \alpha_1 N_{120} + \beta_1 N_\mu + N_r$$

$$N_4 = \alpha_4 N_{120} + \beta_4 N_\mu + N_r$$

$$N_5 = \alpha_5 N_{120} + \beta_5 N_\mu + N_r,$$

where β_5 is small and can be neglected. Given N_1, N_4, and N_5 we then solve for N_{120}.

2. Time factors for background subtraction

To compute a, first find the number N_0 of N^{16} nuclei in the 0^- state at time t by solving the differential equation

$$\frac{dN_0}{dt} = -\lambda_0 N_0 + \lambda_\mu N_{120} e^{-\lambda_\mu t}$$

where

λ_0 = the transition probability for the 0^- level

N_{120} = the total number of 120 keV gammas emitted for all time

λ_μ = the muon disappearance probability.

The solution, with initial condition $N_0 = 0$ at time $t = 0$, is

$$N_0(t) = \frac{\lambda_\mu N_{120}}{\lambda_0 - \lambda_\mu} \left[e^{-\lambda_1 t} - e^{-\lambda_0 t} \right] .$$

However, we want the number of 120 keV gammas emitted in a time interval t_1 to t_2

$$\Delta N = \int_{t_1}^{t_2} \lambda_0 N_0(t)\, dt$$

$$= \frac{\lambda_\mu \lambda_0 N_{120}}{\lambda_\mu - \lambda_0} \left[\frac{e^{-\lambda_\mu t_2} - e^{-\lambda_\mu t_1}}{\lambda_\mu} - \frac{e^{-\lambda_0 t_2} - e^{-\lambda_0 t_1}}{\lambda_0} \right]$$

The time factor is the fraction of the 120 keV gammas that fall into the time interval

$$a = \frac{\Delta N}{N_{120}}$$

$$= \frac{\lambda_\mu \lambda_0}{\lambda_\mu - \lambda_0} \left[\frac{e^{-\lambda_\mu t_2} - e^{-\lambda_\mu t_1}}{\lambda_\mu} - \frac{e^{-\lambda_0 t_2} - e^{-\lambda_0 t_1}}{\lambda_0} \right]$$

where t_2 and t_1 represent the limits of the time interval, e.g. for τ_4, $t_1 = 12.65$ μsec, and $t_2 = 16.65$ μsec.

The time factor β, the fraction of muons decaying between t_1 and t_2, is found in the same manner, but its calculation is easier since only one lifetime is involved. The solution is

$$\beta = \frac{\Delta N}{N_\mu}$$

$$= e^{-\lambda_\mu t_1} - e^{-\lambda_\mu t_2} .$$

3. Time Factor T_{276}

The time factor used in computing the number of 276-keV gamma rays is complicated because of the coincidence system used in this measurement. Consider the decay scheme shown in Fig. 15(a), where a 276-keV gamma ray (γ_{276}) is emitted with a decay constant λ_μ followed by a 120-keV gamma (γ_{120}) emitted with decay constant λ_0. The problem is to find the probability of counting a γ_{120} between t_3 and t_4 that is preceded by a γ_{276} between t_1 and t_2 [see Fig. 15(b)].

Let P_{120} be the probability that a γ_{120} emitted at time t_{120} is preceded by a γ_{276} at time t_{276}

$$P_{120} = A \exp[-(t_{120}-t_{276})\lambda_0]$$

where A is a normalization factor. To find the normalization factor, we require

$$\int_0^{t_{120}} P_{120} dt_{276} = 1,$$

since the γ_{120} must be preceded by a γ_{276}. We then solve for A and find

$$P_{120} = \frac{\lambda_0}{1-e^{-\lambda_0 t_{120}}} \exp[-(t_{120}-t_{276})\lambda_0] .$$

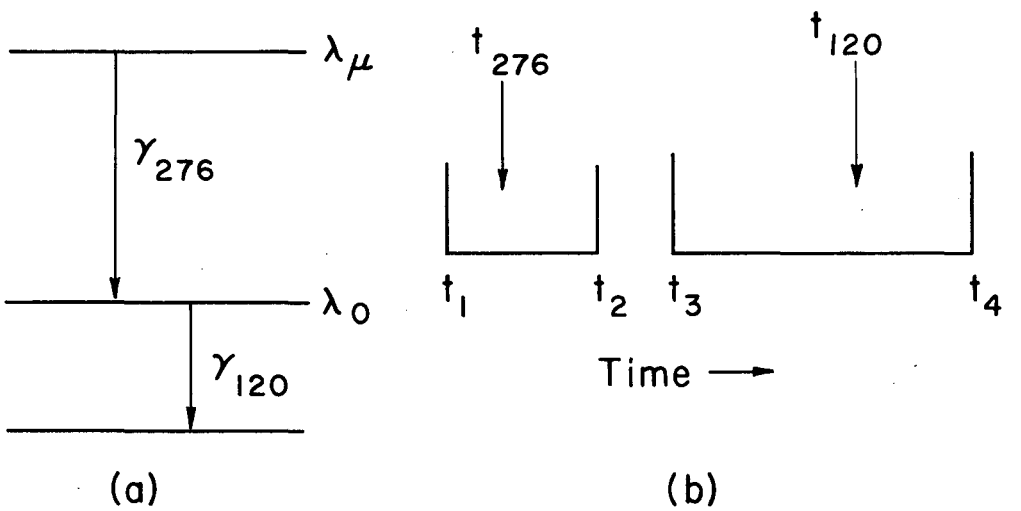

MU-34225

Fig. 15. Diagram showing terms used in the calculation of time factor T_{276}. (a) Decay scheme for coincidence; (b) time sequence in which γ_{276} and γ_{120} are detected.

The probability P that a γ_{120} between t_3 and t_4 is preceded by a γ_{276} at time t_{276} is

$$P = \int_{t_3}^{t_4} P_{120} dt_{120}$$

$$= e^{\lambda_0 t_{276}} \ln\left(\frac{1-e^{-\lambda_0 t_4}}{1-e^{-\lambda_0 t_3}}\right) .$$

The rate at which the γ_{276}'s are emitted is $\lambda_\mu N e^{-\lambda_\mu t}$, where N is the number of initial states. Therefore the probability of finding a γ_{276} at time t_{276}, which is followed by a γ_{120} between t_3 and t_4, is

$$\lambda_\mu N e^{-\lambda_\mu t} P ,$$

and the probability of finding a γ_{276} between t_1 and t_2 followed by a γ_{120} between t_3 and t_4 is

$$\Delta N_{logic} = \int_{t_1}^{t_2} \lambda_\mu N e^{-\lambda_\mu t_{276}} P \, dt_{276}$$

$$= \frac{\lambda_\mu N}{\lambda_0 - \lambda_\mu} \left[e^{(\lambda_0-\lambda_\mu)t_2} - e^{(\lambda_0-\lambda_\mu)t_1}\right] \ln\left(\frac{1-e^{-\lambda_0 t_4}}{1-e^{-\lambda_0 t_3}}\right) .$$

Then the fraction of the γ_{276} that is observed in the coincidence system is

$$T_{276} = \frac{\Delta N_{logic}}{N}$$

$$= \frac{\lambda_\mu}{\lambda_0 - \lambda_\mu} \left[e^{(\lambda_0-\lambda_\mu)t_2} - e^{(\lambda_0-\lambda_\mu)t_1}\right] \ln\left(\frac{1-e^{-\lambda_0 t_4}}{1-e^{-\lambda_0 t_3}}\right)$$

for $t_1 = 0.45$, $t_2 = 4.45$, $t_3 = 4.65$, and $t_4 = 16.65$ μsec, $T_{276} = 0.607$.

B. Evaluation of the Transition Rate

The calculation of the capture rate into the 0^- state of N^{16} begins with the evaluation of the matrix elements $\langle A \| \Xi^{(i)} \| a \rangle$. Using the nuclear model I_G, we evaluate these matrix elements for the particle-particle pairs $2s_{1/2}\ 1p_{1/2}$ and $1d_{3/2}\ 1p_{3/2}$. With $u = 0$, $v = k$, and $\kappa = 1$, the nonzero matrix elements are:

$$\langle 2s_{1/2} \| \Xi^{(2)} \| 1p_{1/2} \rangle = \langle 2s_{1/2} \| \mathcal{O}_{1vu}(\hat{r}, \hat{\sigma}) \| 1p_{1/2} \rangle$$

$$\times \left[S_{110}(1, -1) \int_0^\infty u_{2,0} g_1 G_{-1} u_{1,1} r^2 \, dr \right.$$

$$\left. - S_{110}(-1, +1) \int_0^\infty u_{2,0} f_1 F_{-1} u_{1,1} r^2 \, dr \right] .$$

Using $b = 1.75$ f, $q = 93.5$ MeV/c, and the Hermite-Gauss numerical integration procedure, we obtain

$$\langle 2s_{1/2} \| \Xi^{(2)} \| 1p_{1/2} \rangle = \sqrt{\frac{3}{8\pi^2}} \left[-\sqrt{\frac{2}{3}} \ (-8.01) - \sqrt{\frac{2}{3}} \ (0.181) \right] = +1.25$$

in the same way we compute

$$\langle 1d_{3/2} \| \Xi^{(2)} \| 1p_{3/2} \rangle = \frac{\sqrt{3}}{2\pi} \left[\left(-\sqrt{\frac{2}{3}} \right) (14.68) - \sqrt{\frac{2}{3}} \ (-0.840) \right] = -3.11$$

$$\langle 2s_{1/2} || \Xi^{(6)} || 1p_{1/2} \rangle = (-)^{1+1/2+1/2} \sqrt{6} \sum_{\ell'=0,\,2} \langle 0 || \mathcal{O}_{0vu}(\hat{r}) || \ell' \rangle$$

$$\times \begin{Bmatrix} 1/2 & 1/2 & \ell' \\ 1 & \ell_a & 1/2 \end{Bmatrix} \left[S_{000}(-1,-1) \int_0^\infty u_{2,0} f_1 G_{-1} D_{\ell'} u_{1,1} r^2 \, dr \right.$$

$$\left. + S_{000}(1,1) \int_0^\infty u_{2,0} g_1 F_{-1} D_{\ell'} u_{1,1} r^2 \, dr \right]$$

$$D_2 = \sqrt{\frac{2}{3}} \left(\frac{d}{dr} - \frac{1}{r} \right)$$

$$D_0 = \sqrt{\frac{1}{3}} \left(\frac{d}{dr} + \frac{2}{r} \right)$$

$$\langle 2s_{1/2} || \Xi^{(6)} || 1p_{1/2} \rangle = \sqrt{6} \sqrt{\frac{1}{8\pi^2}} \frac{1}{\sqrt{6}} \left[\sqrt{2}(-7996) + (-\sqrt{2})(66.1) \right] = -1283$$

$$\langle 1d_{3/2} || \Xi^{(6)} || 1p_{3/2} \rangle = (-)^{1+1/2+3/2} \sqrt{6} \frac{1}{2\pi} \frac{1}{2\sqrt{3}} \left[\sqrt{2}(-1.38 \times 10^4) + (-\sqrt{2})(231) \right]$$

$$= +2233,$$

$$\langle 2s_{1/2} || \Xi^{(7)} || 1p_{1/2} \rangle = \langle 2s_{1/2} || \mathcal{O}_{110}(\hat{r}, \vec{\sigma}) || 1p_{1/2} \rangle$$

$$\times \left[S_{000}(-1,-1) \int_0^\infty u_{2,0} D_+ f_1 G_{-1} u_{1,1} r^2 \, dr \right.$$

$$\left. + \; S_{000}(1,1) \int_0^\infty u_{2,0} D_+ g_1 F_{-1} u_{1,1} r^2 \, dr \right]$$

$$= \sqrt{\frac{3}{8\pi^2}} \left[\sqrt{2}(1535) + (-\sqrt{2})(-3.83) \right]$$

$$= 424.2 \, .$$

$$\langle 1d_{3/2} || \Xi^{(7)} || 1p_{3/2} \rangle = \frac{\sqrt{3}}{2\pi} \left[\sqrt{2}(-3034) + (-\sqrt{2})(-29.6) \right] = -1171$$

$$\langle 2s_{1/2} || \Xi^{(8)} || 1p_{1/2} \rangle = \sqrt{\frac{3}{8\pi^2}} \left[\sqrt{2}(1535) - (-\sqrt{2})(-3.83) \right] = 422.1$$

$$\langle 1d_{3/2} || \Xi^{(8)} || 1p_{3/2} \rangle = \frac{\sqrt{3}}{2\pi} \left[\sqrt{2}(-3034) - (-\sqrt{2})(-29.6) \right] = -1194$$

Substituting the amplitudes of Table VII into Eq. (10), we find

$$X_{2s\ 1p} = -0.999$$

$$X_{1d\ 1p} = -0.055.$$

Using Eqs. (11) and (12), we find that

$$\mathcal{M}^{(2)} = \langle f || \Xi^{(2)} || 0 \rangle$$

$$= (-0.999)(1.25) + (-0.055)(-3.11)$$

$$= -1.05$$

$$\mathcal{M}^{(6)} = 1136$$

$$\mathcal{M}^{(7)} = -350$$

$$\mathcal{M}^{(8)} = -346.$$

Letting $C_P = 7\ C_A$, we obtain for the coupling constants in natural units

$$C^{(2)} = 3.55 \times 10^{-12}$$

$$C^{(6)} = -1.93 \times 10^{-15}$$

$$C^{(7)} = 5.58 \times 10^{-16}$$

$$C^{(8)} = -3.91 \times 10^{-15}.$$

These matrix elements and coupling constants are substituted into Eq. (7) to give

$$\left|\langle f|H|0\rangle\right|^2_{avg} = 1.14\times10^{-23}.$$

With a value of q = 183 (natural units), we find the transition rate from Eq. (5) to be

$$\lambda = (2\pi)\,(1.14\times10^{-23})\,(183)^2\,(0.994)\,\frac{1}{1.288\times10^{-21}}$$

$$= 1.83\times10^{3}\ \text{sec}^{-1}$$

where we have used $\frac{\hbar}{m_e c^2} = 1.288\times10^{-21}$ sec.

FOOTNOTES AND REFERENCES

1. I. S. Shapiro and L. D. Blokhintsev, Capture of μ^- Mesons by the O^{16} Nucleus, (English trans.) Soviet Phys. -JETP 12, 775 (1961).
2. M. L. Goldberger and S. B. Treiman, Form Factors of β Decay and μ Capture, Phys. Rev. 111, 354 (1958).
3. K. C. Chou, On the Pseudoscalar Current and Lepton Decays of Baryons and Mesons, (English trans.) Soviet Phys. -JETP 12, 492 (1961).
4. G. Feinberg and L. M. Lederman, The Physics of Muons and Muon Neutrinos, in Annual Reviews of Nuclear Science, Vol. 13 (1963).
5. J. D. Jackson, Weak Interactions, in Elementary Particle Physics and Field Theory (Brandeis Lectures, Brandeis University, 1962), Vol. 1.
6. J. C. Taylor, The Magnitude of the Induced Pseudoscalar Term, Phys. Letters 11, 77 (1964).
7. For example, see the review article in Ref. 4, p. 431.
8. W. W. Givens, T. W. Bonner, S. H. Fang, R. C. Bearse, and A. A. Rollefson, Gamma Radiations from Excited States of N^{16}, Nucl. Phys. 46, 504 (1963).
9. R. Cohen, S. Devons, and A. Kanaris, Muon Capture in Oxygen, Phys. Rev. Letters 11, 134 (1963); also submitted to Nucl. Phys.
10. Robert J. Esterling, Measurements of the Muon Capture Rate in He^3 and He^4 (Ph. D. Thesis), UCRL-11004, April 1964.
11. F. Ajzenberg-Selove and T. Lauritsen, Energy Levels of Light Nuclei. VI, Nucl. Phys. 11, 203 (1959).
12. K. W. Ford and J. G. Wills, Calculated Properties of Mu-Mesic Atoms, Los Alamos Scientific Laboratory Report LAMS-2387, March 1960; Nucl. Phys. 35, 295 (1962).
13. Y. Eisenberg and D. Kessler, On the μ-Mesonic Atom, Nuovo Cimento 19, 1195 (1961).
14. E. Fermi and E. Teller, The Capture of Negative Mesotrons in Matter, Phys. Rev. 72, 399 (1947).

15. D. Strominger, J. M. Hollander, and G. T. Seaborg, Table of Isotopes, Rev. Mod. Phys. 30, 585 (1958).

16. I. Duck, Muon Capture in the Shell Model (Ph. D. Thesis), California Institute of Technology, 1961; Nucl. Phys. 35, 27 (1962).

17. J. P. Elliott and B. H. Flowers, The Odd-Partiy States of O^{16} and N^{16}, Proc. Roy. Soc. (London), A242, 57 (1957).

18. Vincent Gillet, Theorie des Spectres des Noyaux a Couches Completes (Ph. D. Thesis), Centre d' Etudes Nucléaires de Saclay Rapport CEA-2177, 1962 (unpublished); Nucl. Phys. 51, 410 (1964).

19. M. Morita and A. Fujii, Theory of Allowed and Forbidden Transitions in Muon Capture Reactions, Phys. Rev. 118, 606 (1960).

20. S. Weinberg, Charge Symmetry of Weak Interactions, Phys. Rev. 112, 1375 (1958).

21. M. Deutsch and O. Kofoed-Hansen, Beta Rays, in Experimental Nuclear Physics, E. Segrè, Ed. (John Wiley and Sons, Inc., New York, 1959), Vol. III, p. 514.

22. G. Flamand and K. W. Ford, Muon Capture by C^{12} and Beta Decay of B^{12}, Phys. Rev. 116, 1591 (1959).

23. G. E. Pustovalov, Energy Levels and Approximate Wave Functions of Mesic Atoms, (English trans.) Soviet Phys. --JETP 9, 1288 (1959).

24. K. W. Ford (Department of Physics, Brandeis University), private communication, May 1964.

25. M. Morita and R. Morita, Possible G-Parity Nonconservation in Muon Capture Reactions, Research Institute of Fundamental Physics, Kyoto University, Kyoto, Japan, Report RIPF-37, May 1964 (submitted to J. Phys. Soc. Japan).

26. A. R. Edmonds, Angular Momentum in Quantum Mechanics (Princeton University Press, Princeton, N. J., 1957).

27. J. S. Bell, Particle-Hole Conjugation in the Shell Model, Nucl. Phys. 12, 117 (1959).

28. E. J. Maier, R. M. Edelstein, and R. T. Siegel, Measurement of the Reaction $\mu^- + C^{12} \rightarrow B^{12} + \nu$, Phys. Rev. 133, B663 (1964).

29. L. R. B. Elton, Nuclear Sizes (Oxford University Press, London, 1961).

30. E. G. Beltrametti and L. A. Radicati, μ^- Capture in Light Nuclei, Nuovo Cimento 11, 793 (1959).

31. Torleif Ericson (CERN, Geneva), private communication, June 1964.

32. Nicola Cabibbo (Lawrence Radiation Laboratory), private communication, April 1964.

33. John O. Rasmussen, Jr., (Lawrence Radiation Laboratory), private communication, April 1964.

34. Hans J. Mang (Lawrence Radiation Laboratory), private communication, April 1964.

35. J. D. McCullen, B. F. Bayman, and L. Zamick, Spectroscopy in the Nuclear $1f_{7/2}$ Shell, Phys. Rev. 134, B515 (1964).